UNIVERSITÀ
DEGLI STUDI
DI BRESCIA

DOTTORATO DI RICERCA IN TECHNOLOGY FOR HEALTH

MED/28 Malattie Odontostomatologiche

XXXIII CICLO

DISTRIBUTION ON THE FACE OF THE FORCES RELATED TO THE USE OF CONTINUOUS POSITIVE AIRWAY PRESSURE MASK AND POSSIBLE EFFECTS ON CRANIOFACIAL GROWTH

DOTTORANDO:

Dott. Lorenzo Svanetti

RELATORE:

Professor Corrado Paganelli

CORRELATORE:

Professor Nicola Francesco Lopomo

I. Abstract

Obstructive sleep apnoea (OSA) is a breathing disorder characterised by repeated episodes of prolonged upper airway obstruction and/or intermittent complete obstruction that disrupts normal sleep patterns. Continuous positive airway pressure (CPAP) is a respiratory ventilation method used in the treatment of OSA. However, the forces applied by the CPAP mask in growing subjects may affect facial development, especially of the maxillary complex. Therefore, the objective of the present work was to understand how the pressure of the CPAP mask is distributed on the face, in order to provide information to clinicians for optimising treatments and helping to develop more functional CPAP mask designs.

A laboratory experiment was conducted using a CPAP mask that was applied with a mechanical testing machine on a rigid phantom head, either with perpendicular forces or indirectly via the headgear bands of the mask. Test were repeated with different magnitude of force (5 N, 10 N, 15 N, and 20 N). During the experiment, pressure mapping sensors were applied on the facial surface in four areas (forehead, nasal bridge zygomatic area, and maxilla).

A virtual model was created by 3D scanning the CPAP mask and the phantom head. The headgear securing the mask on the face was also virtually modelled. A finite element analysis (FEA) was conducted by applying the CPAP mask on the face, both with direct perpendicular loading and indirect loading through the headgear, with forces up to 20 N. The distribution of forces and pressures on the face was calculated by FEA and results were analysed in different areas of the face.

In general, the comparison of each area between the FEA and the laboratory experiment showed similar results. However, the most critical area seemed to be the maxilla, which showed a smaller loading in the FEA. Overall, the applied pressures were slightly lower in the FEA,

but still within a similar order of magnitude. Such differences may vary based on the position of the mask adopted in the FEA. In particular, in the FEA obtained with indirect loading through the headgear, the contact area shifted towards the forehead.

The simulation and experimental tests showed that the CPAP mask can exert forces that are not uniformly distributed on the face. Interpretation of these mechanical data with respect to craniofacial biomechanics should be considered by clinicians in order to obtain the best compromise between the CPAP treatment performance - in terms of ventilation - and the possible side-effects on growing craniofacial structures.

[TRADUZIONE DELL'ABSTRACT]

[L'apnea ostruttiva del sonno (OSA) è un disturbo respiratorio caratterizzato da ripetuti episodi di ostruzione prolungata delle vie aeree superiori e/o ostruzione completa intermittente che interrompe i normali ritmi del sonno. La pressione positiva continua delle vie aeree (CPAP) è un metodo di ventilazione respiratoria utilizzato nel trattamento dell'OSA. Tuttavia, le forze applicate dalla maschera CPAP nei soggetti in crescita possono influenzare lo sviluppo del viso, in particolare del complesso mascellare. Pertanto, l'obiettivo del presente lavoro è stato capire come la pressione della maschera CPAP venisse distribuita sul viso, al fine di fornire informazioni ai medici per ottimizzare i trattamenti ed aiutare a sviluppare modelli di maschere CPAP più funzionali.

È stato condotto un esperimento di laboratorio utilizzando una maschera CPAP applicata con una macchina per prove meccaniche su un modello di testa rigida, con forze perpendicolari, o indirettamente tramite le fasce del reggi-maschera. I test sono stati ripetuti con diverse intensità di forza (5 N, 10 N, 15 N e 20 N). Durante l'esperimento sono stati applicati sensori di mappatura della pressione sulla superficie facciale in quattro aree (fronte, area zigomatica, del ponte nasale, e la mascella).

È stato creato un modello virtuale scansionando in 3D della maschera CPAP e della testa. Anche il regi-maschera che fissa la maschera sul viso è stato modellato virtualmente. È stata condotta un'analisi agli elementi finiti (FEA) applicando la maschera CPAP sul viso, sia con carico perpendicolare diretto che con carico indiretto attraverso il reggi-maschera, con forze fino a 20 N. La distribuzione delle forze e delle pressioni sul viso è stata calcolata tramite la FEA ed i risultati sono stati analizzati nelle diverse aree del viso.

In generale, il confronto di ciascuna area tra la FEA e l'esperimento di laboratorio ha mostrato risultati simili. Tuttavia, l'area più critica è risultata essere la mascella, che mostrava un carico più piccolo nella FEA. Nel complesso, le pressioni applicate erano leggermente inferiori nella FEA, ma di un ordine di grandezza simile. Tali differenze possono variare in base alla posizione della maschera adottata nella FEA. In particolare, nella FEA ottenuta con carico indiretto tramite il reggi-maschera, l'area di contatto si è spostata verso la fronte.

La simulazione e le prove sperimentali hanno dimostrato che la maschera CPAP può esercitare forze non uniformemente distribuite sul viso. L'interpretazione di questi dati meccanici rispetto alla biomeccanica craniofacciale va interpretata valutare criticamente quale possa essere il miglior compromesso tra le prestazioni del trattamento CPAP - in termini di ventilazione - ed i possibili effetti collaterali sulle strutture cranio-facciali di soggetti in crescita.]

II. Table of contents

III. List of abbreviations:

- Automatic positive airway pressure (APAP)
- Bi-level positive airway pressure (BiPAP)
- Computer-aided design (CAD)
- Continuous positive airway pressure (CPAP)
- Finite element analysis (FEA)
- Initial graphics exchange specification (IGES)
- Mandibular advancement device (MAD)
- Non-invasive positive pressure ventilation (NPPV)
- Obstructive sleep apnoea (OSA)
- Polycarbonate (PC)
- Polysomnography (PSG)
- Polyvinyl chloride (PVC)
- Sleep disordered breathing (SDB)
- Stainless steel (SS)
- Standard triangulation language (STL)
- Three-dimensional (3D)
- Vinyl-methyl silicone rubber (VMQ)

1. INTRODUCTION

There are two main aspects that should be considered in the present investigation: one is the knowledge about the disease that is treated with the continuous positive airway pressure (CPAP), i.e the obstructive sleep apnoea (OSA), and the other is related to the consequences of the forces exerted by such device on the face of a growing patient, especially with regard to the upper and lower jaw. This thesis will focus on the mechanical and virtual simulation of the forces exerted the CPAP on the face.

1.1 Obstructive sleep apnoea

Sleep disordered breathing (SDB) is characterised by abnormal respiration during sleep *(Jennum 2009).* SDB ranges from intermittent partial obstruction of the upper airway without sleep disturbance (snoring), to frequent apnoeas associated with repetitive hypoxaemia and arousals leading to sleep disruption and daytime symptoms *(Jennum, 2009).* OSA is a severe SDB that consists of recurrent episodes of complete (apnoea) or partial (hypopnea) obstruction of the upper airway during sleep, caused by anatomical and/or functional alteration of the upper airways *(Doff, 2010)*. OSA is accompanied by desaturation of oxygen and awakenings, causing a multitude of symptoms that include sleep fragmentation, daytime symptoms, cardiovascular morbidities, and cognitive impairment *(Jennum, 2009)*. In particular, OSA results in greater respiratory effort with reductions in oxyhaemoglobin saturation, fluctuations in heart rate, and increased systemic and pulmonary blood pressure *(Tsuda, 2010)*. In the daytime, children with OSA may also show hyperactivity, and the severity of the disorder correlates with learning difficulties, reduced attention span, and neuro-behavioural problems *(Deng, 2012; Fauroux, 2005)*. The prevalence of OSA is higher in obese patients and in those with craniofacial malformations such as Down syndrome *(Jennum, 2009).* In fact, craniofacial abnormalities may negatively affect the patency of the upper airway, increasing the risk of a child having OSA (*Chan, 2004)*.

1.2 Continuous positive airway pressure

The use of positive air pressure has become widely applied in several systemic disorders, including OSA. The air can be administered at variable pressures through automatic positive airway pressure (APAP) ventilators *(Massie, 2003)*, or continuous positive airway pressure (CPAP) ventilators *(Mortimore, 1998)*. The CPAP is composed of a compressor that increases the air pressure (blower), a tube that connects the blower to the mask, and the mask connecting the device to the airway of the patient. The CPAP is worn by the patient mainly during night time, which allows the patient to breathe spontaneously while the ventilator mechanically dispenses air at one level of pressure, leaving the exhalation of the patient passive allowing the escape of carbon dioxide via specific areas of the mask *(Oto, 2013).* The nasal CPAP masks can be either nasal or oro-nasal, and present different shapes for a better adaptation to the face *(Krieger, 1992).* They are equipped with a headgear constituted by elastic bands that keep the mask in the correct position *(Tsuda, 2010).* The CPAP device allows the elimination of the blockage of the airways created by the collapse of the muscles, without causing excessive disturbances during sleep *(Mcardle, 1999)*. In patients affected by OSA, CPAP devices are highly effective and they represent the gold standard treatment *(Mortimore, 1998)*. However, sometimes only partial improvement occurs *(Villa, 2002)*. Furthermore, they do not have a permanent effect and, if the use is stopped, symptoms often return immediately because the treatment is not curative *(Mcardle, 1999).* In general, the administration of the treatment should be of 8 to 10 hours per night *(Force, 2008)* and, in some cases, daytime application is prescribed as well *(Force, 2008)*. Nevertheless, the actual use can be variable depending on the compliance of the patient, which is estimated to range between 5 and 8 hours per night *(Force, 2008)*. The CPAP ventilator supplies air at the prescribed pressure that is called titrated pressure, which is the air pressure at which most apnoeas and hypopneas are

prevented. During treatment, the air is delivered at values ranging from few cm of H_2O to 20 cm of H_2O, with some authors reporting titration reaching 30 cm of H_2O *(Force, 2008)*. The required pressure is usually determined by a physician after analysing a polysomnography (PSG) performed during night in a sleep laboratory.

Possible compliance problems may be related to intolerance to the mask by the patient due to claustrophobia, damages to the facial skin, and instability of the mask position. Further, technical limitations may include air leakage. For this reason, CPAP masks are available in different sizes and shapes, and patients may need to try different models before finding the one that best fits to their face, and is also suitable for their needs, habits and sensations.

1.3 Dental and skeletal side effects of CPAP mask

CPAP masks may have adverse effects on the dentition. For example, in adults with OSA the use of nasal CPAP for two years for at least 4 hours/day may be associated with changes in the dental arches relationship, and the prominence of the upper incisors may result retruded compared to the lower incisors *(Tsuda, 2010)*. Mandibular advancement devices (MAD) are oral appliances that reposition the mandible and the tongue anteriorly, and they can be used for the treatment of OSA *(Incerti Parenti, 2020; Bartolucci ML, 2016)*. By using a mandibular advancement device (MAD) compared with CPAP for the treatment of OSA, after two years the CPAP was associated with a decrease in overbite, while smaller dental effects were present with the oral appliance *(Doff, 2010)*.

CPAP effects can also be skeletal, with primary involvement of the maxilla, and risk of facial flattening and maxillary retrusion were reported with a use of mask greater than 10 hours/day *(Fauroux, 2005)*. Facial flattening and convex skeletal profile with maxillary hypoplasia and mandibular protrusion were also reported in a child using a bilevel positive airway pressure (BiPAP) mask since the age of 9 months *(Villa, 2002)*. Children with OSA using nasal CPAP mask were reported to show severe depression of the peri-nasal region and convex skeletal profile *(Li, 2000)*. Similarly, after two years of CPAP use in adults with OSA, compared to MAD, mandibular protrusion was reported *(Doff, 2010)*, and the use of nasal CPAP for two years for at least 4 hours/day was associated with reduced maxillary and mandibular prominence *(Tsuda, 2010)*.

The use of a mask may also affects soft tissues, which may be particularly evident in children. In fact, treatment for at least one month and for at least 6 hours/day was associated

with skin injuries on the forehead and glabella, in some cases associated with erythema and skin necrosis, with a favourable effect if changing to a custom-made mask.

1.4 Dental and skeletal characteristics of obstructive sleep apnoea patients

Dentoskeletal and upper airway characteristics are commonly assessed with lateral cephalometric radiography *(Savoldi et al., 2020b)*. Especially, maxillary hypoplasia has particular relevance in the onset of mid-face deformities *(Savoldi et al., 2020 c)*. Besides the side effects attributable to the CPAP therapy, OSA patients are already affected by dental and skeletal malformations that may be worsened by prolonged use of CPAP mask. Skeletally, children with OSA are often characterized by retruded jaws and elongated lower third of the face *(Flores-Mir, 2013; Deng, 2012)*. Dentally, children with OSA have narrower dental arches *(Smith, 2016)*, increased overjet, reduced overbite, higher prevalence of anterior open bite and class II, and dental crowding compared to controls *(Pirilä-Parkkinen, 2008)*. In children with upper airway obstruction, the maxillary may be smaller, and the length of the lower dental arch was shorter, the palatal vault was higher, and lateral cross-bite was more frequent compared to controls *(Löfstrand-Tideström, 1999)*. Lateral cross-bite is also more common in children snoring regularly, together with a narrower upper jaw than those children who do not snore *(Hultcrantz, 2009)*. Conversely, adults with OSA seem to have altered cephalometric parameters compared to adults with snoring, but no altered dental parameters *(Frohberg, 1995)*.

1.5 Technical review of the literature

At present, little information is available in the published literature about the forces or pressures exerted on the face by the CPAP mask, and potential side effects with respect to facial development of growing individuals are of recent interest. In fact, attention has been mainly directed towards limiting the air leakage of the CPAP mask, and not to the forces used to stabilise it on the face. Nevertheless, recent studies have described the pressures generated by the CPAP mask on facial areas such as the nasal bridge, ranging from 60 to 75 mm of Hg according to one study *(Brill, 2017a)*, and from 47 to 92 mm of Hg according to other authors *(Brill, 2017b)*. In addition, forces of 0.5 N on the cheeks, 2 N on the nasal bridge, and 4 N on the chin have been reported by others *(Cohen, 2018)*. Still, only limited areas interested by CPAP mask pressures have been analysed, and a comprehensive assessment of the overall pressures and forces exerted by the mask is needed.

More information is available in the literature regarding the amount of force that may generate orthopaedic effects on the facial skeleton of a growing patient. Most of this knowledge comes from orthodontic studies about the use of headgears, which consist of devices anchored to the cranial vault that transfer compressive forces on the maxilla to limit its growth and correct skeletal class II facial deformities. For example, it has been shown that a posteriorly directed force of approximately 5 N applied on each side on the maxillary molars may restrain the anterior development of the maxillary complex *(Braun, 2004)*. Clinically, by setting the headgear at approximately 5 N per side, for a total force of 10 N, the clinically detected total force ranged between 2 N to 12 N *(Johnson, 1999)*. Accordingly, the activation range of the headgear revealed forces from 2 N to 11 N *(Lyons, 2002)*. Although the optimal force required for generating skeletal growth modifications is unknown, it is reasonable to assume that a force between 2 N and 12 N may induce growth modifications in young patients. In fact, previous

studies that developed finite element analysis (FEA) simulations of such craniofacial effects, uniformly adopted forces of 10 N *(Gautam, 2009, Tanne, 1993, Tanne, 1996)*. Unfortunately, the available data are limited to the maxilla and, to the best of our knowledge, no information is available in the published literature about the forces required to modify the growth of other facial bones.

1.6 Objectives

The objective of the present work was to understand the effects of CPAP procedure on the development of mid-face deformities, by quantitatively estimating the distribution of the forces exerted by the mask on the face. Such knowledge is, in fact, essential to allow a CPAP treatment that minimises the onset of these defects. This is particularly relevant in growing subjects affected by OSA, where these malformations can worsen already unfavourable anatomical characteristics. Thus, optimizing the mask design and its application according to the facial type of the patient is important.

1.7 Thesis outline

The present thesis used a phantom head and a CPAP for developing laboratory tests and FEA models. Mechanical testing of CPAP mask materials was carried out preliminarily to FEA simulations, and the FEA was validated by comparison with results obtained from pressure-mapping sensors. Different scenarios were considered, including forces applied either perpendicularly or through a headgear, and different force magnitudes.

The FEA simulation data and the laboratory results were presented and compared. Lastly, the discussion will further explain the physiology of craniofacial biomechanics and the effects of CPAP forces, focusing on clinical considerations about the facial structures.

2. MATERIALS AND METHODS

In order to understand the distribution of the forces generated by the CPAP mask on the face, a phantom head was used to simulate the face of a patient and a real CPAP mask was applied on it. First the materials constituting the CPAP mask received mechanical characterisation, which were necessary for FEA analysis.

*Pressure-mapping sensors were applied on the phantom head, their position was registered in 3D, and they were calibrated. Eventually, the FEA models were validated by means of two simplified situations: one with the phantom head and one with all components. Finally, a full FEA model including the headgear provided results to be compared with the analogous laboratory test (**Figure 1**).*

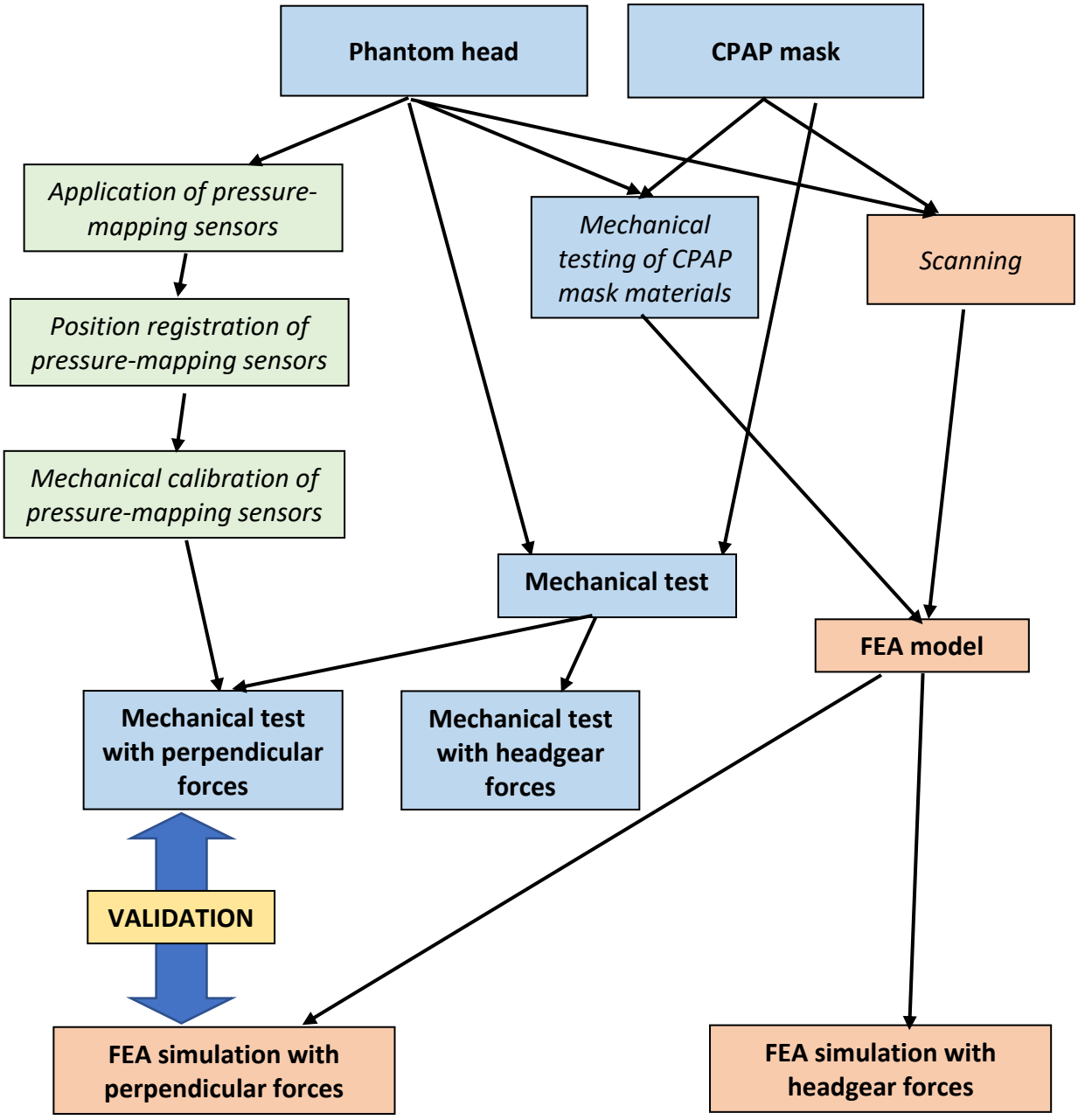

Figure 1: Flowchart of the thesis organisation.

2.1 Phantom head

A hallow polyvinyl chloride (PVC) phantom head was purchased and filled with extra-strong (class IV) dental plaster. The head simulated a young male presenting normal facial profile (skeletal class I) (**Figure 2**).

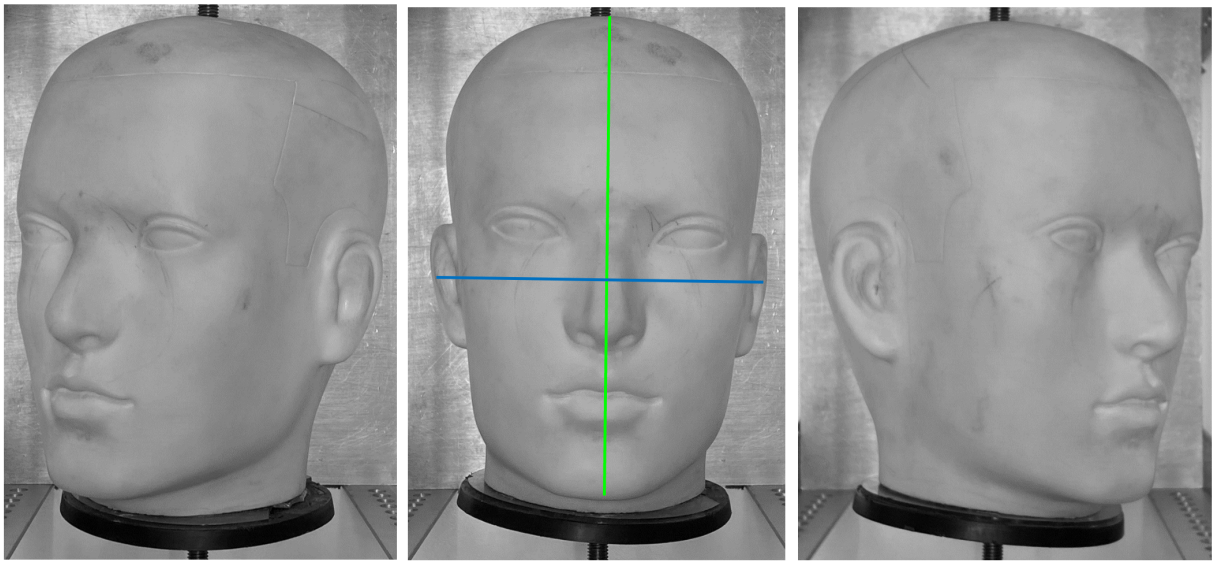

Figure 2: Phantom head used for the experiment (210 mm height from chin to top of the head, 160 mm width from ear to ear).

The head was mounted on a stainless-steel threaded rod connected to a custom-made frame allowing inclination and rotation adjustments, to properly position the head during mechanical testing. The weight of the head and frame system was 11.5 kg (**Figure 3**).

Figure 3: Custom-made aluminium frame holding the head during laboratory tests. The frame (41.0 cm height, 30.5 cm antero-posterior width, and 25.5 cm latero-lateral depth) consisted of aluminium bars stabilised with SS screws and bolts on an aluminium base.

For the FEA, the phantom head was scanned with a laboratory 3D optical laser device (Open Technologies, croNos3D) and acquired as point cloud (**Figure 4**).

Figure 4: Scanning of the phantom head (upper) and 3D image reconstruction of the same phantom head (lower). Optical scanner that was used.

The data were opened with graphical software (Geomagic Studio, v2014, 3D Systems), converted in standard triangulation language (STL) format, and transformed in a virtual solid object, which geometry was cleaned and simplified. Lastly, the virtual object was opened with graphical software (Abaqus/CAE, Dassault Systèmes, 2015, Simulia), converted in Standard ACIS Text format (SAT), and refined via computer-aided design (CAD) function (reduction of short edges and small angles) (**Figure 5**).

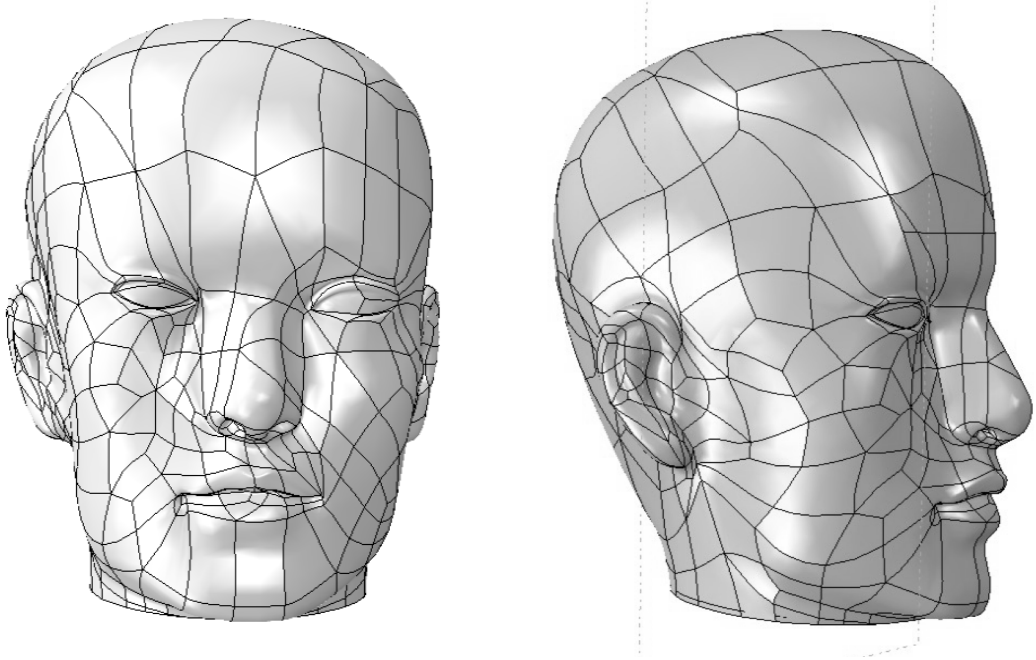

Figure 5: Phantom head scan obtained and refined.

2.2 CPAP mask

A commercially available medium size nasal CPAP mask was used (iVolve N2, BMC Medical, P. R. of China). Such mask was composed by a transparent polycarbonate (PC) rigid frame (with a hole for connecting the pipe delivering the pressurised air) that supported a vinyl-methyl silicone rubber (VMQ) cushion for sealing the interface between the mask and the skin. An extension of the frame connected a forehead support also provided with a VMQ cushion to avoid skin damages (**Figure 6**).

Figure 6: CPAP mask used for the experiment (80 mm width top and 60 mm width bottom × 55 mm thickness with silicon and 37 mm thickness without silicon × 120 mm length).

For the FEA, the mask was sprayed with opaque powder (to avoid the transparent PC to interfere with the scanning procedures), and scanned with a laboratory 3D optical laser device (Open Technologies, croNos3D) and acquired as point cloud (**Figure 7**).

Figure 7: Scanning of the CPAP mask (upper) and 3D image reconstruction of the same CPAP mask (lower). Optical scanner that was used.

The data were opened with graphical software (Geomagic Studio, v2014, 3D Systems), converted in standard triangulation language (STL) format, and transformed in a virtual solid object, which geometry was cleaned and simplified. Lastly, the virtual object was opened with graphical software (Abaqus/CAE, Dassault Systèmes, 2015, Simulia), converted in Standard ACIS Text format (SAT), and refined via computer-aided design (CAD) function (reduction of short edges and small angles) (**Figure 8**).

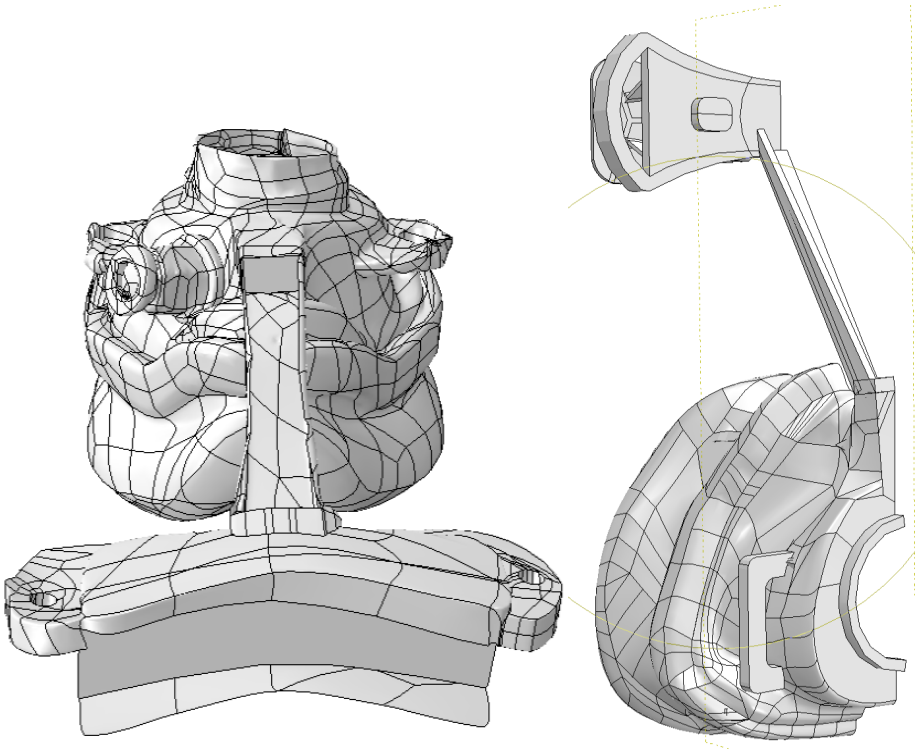

Figure 8: CPAP mask scan obtained and refined.

2.3 Headgear bands

The CPAP mask presented a headgear consisting of two bands (20.0 mm width, and 2.5 mm thickness for terminal parts or 1.7 mm thickness for the others, as terminal parts were folded to allow to tighten the headgear), one upper and one lower. The bands were made of one layer of unbroken loop fabric (UBL) on the outer surface, one layer of styrene butadiene copolymeric rubber (SBR) in the middle, and one layer of nylon (70D) on the inner surface. In general, the material could be described as neoprene/nylon. Four Velcro connectors were attached to the extremity of each band, which allowed connection to the PC frame at the forehead level and at the nasal level (symmetrically on both sides). The Velcro connectors allowed to regulate the length of the neoprene/nylon bands for tightening the mask on the face (**Figure 9**).

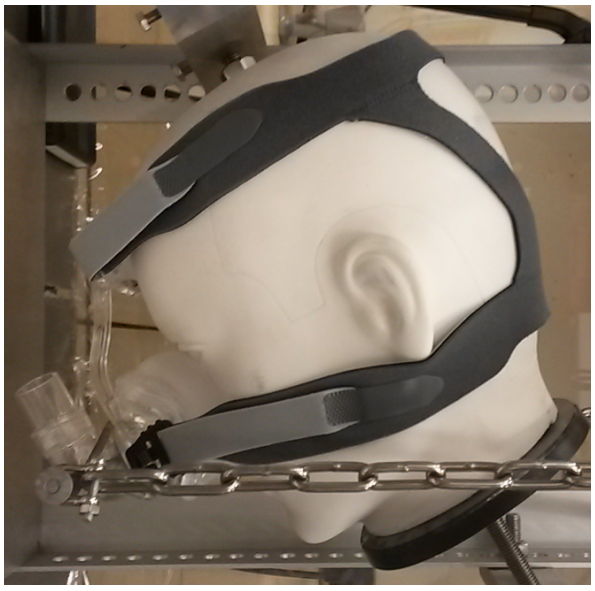

Figure 9: The system consisting of the phantom head stabilised on the metal frame, with the CPAP mask positioned and stabilised with the headgear bands.

For the FEA, a 3D model of the bands of the headgear was manually created with CAD modulus based on the measurement of the real object (Abaqus/CAE, Dassault Systèmes, 2015, Simulia) (**Figure 10**).

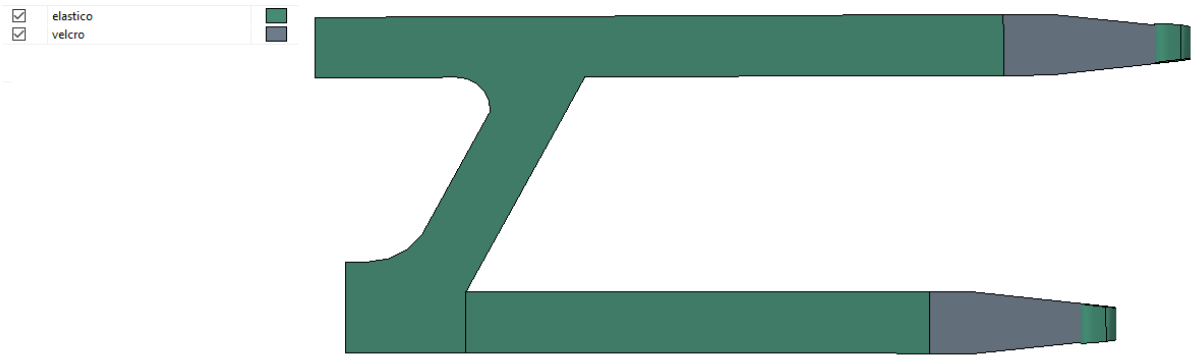

Figure 10: 3D model of the rubber band of the headgear.

2.4 Mechanical testing of CPAP mask and headgear materials

A CPAP mask (which was the same model of the scanned mask) was used for the preparation of the specimens. Tests were performed with mechanical testing machine (Instron® 5848 Micro Tester, Norwood, MA, USA) with static load cell of ± 2,000 N, at room temperature (25 °C ± 1 °C) and room humidity (65% ± 1%), measuring time (s), displacement (mm), and force (N) under either imposed load or imposed displacement. The precision of the testing machine was ± 0.5 μm up to 0.25 mm (for PC testing), and ± 2.5 μm up to 10.00 mm (for VMQ testing) *(Instron)*. Raw data were filtered excluding those outside the range of interest of each test (either beyond 20 N of forces or beyond 20 % of deformation), and force-displacement curves were generated (Microsoft Excel©, Microsoft, WA, USA).

For obtaining mechanical data for the FEA, the PC was tested in uniaxial compression positioning a specimen on a stainless steel (SS) flat plate and pressed with the head of the machine mounting a SS flat tip (20.0 × 26.0 mm). The specimen consisted of a hollow PC cylinder (20.0 mm height × 1.5 mm thickness × 22.0 mm Ø) that was cut with a high-speed cutting disk from the connection pipe of the mask. The tests was performed at a speed of 0.33 mm/min up to 20 N of force (**Figure 11**).

For obtaining mechanical data for the FEA, PC was also tested in uniaxial tension by locking the terminal parts of the specimen in SS clamps. The specimen (4.0 mm width × 1.5 mm thickness × 7.0 mm length) consisted of a PC beam cut with a high-speed cutting disk from a relatively flat area of the mask. After drilling a 1.0 mm hole at the terminal parts and inserting a glass-fibre post, the extremities were embedded in self-curing acrylic resin to uniformly distribute the strain within the specimen and reduce the slippage during testing. Test was performed at a speed of 1.0 mm/min up to 20 N of force (**Figure 11**).

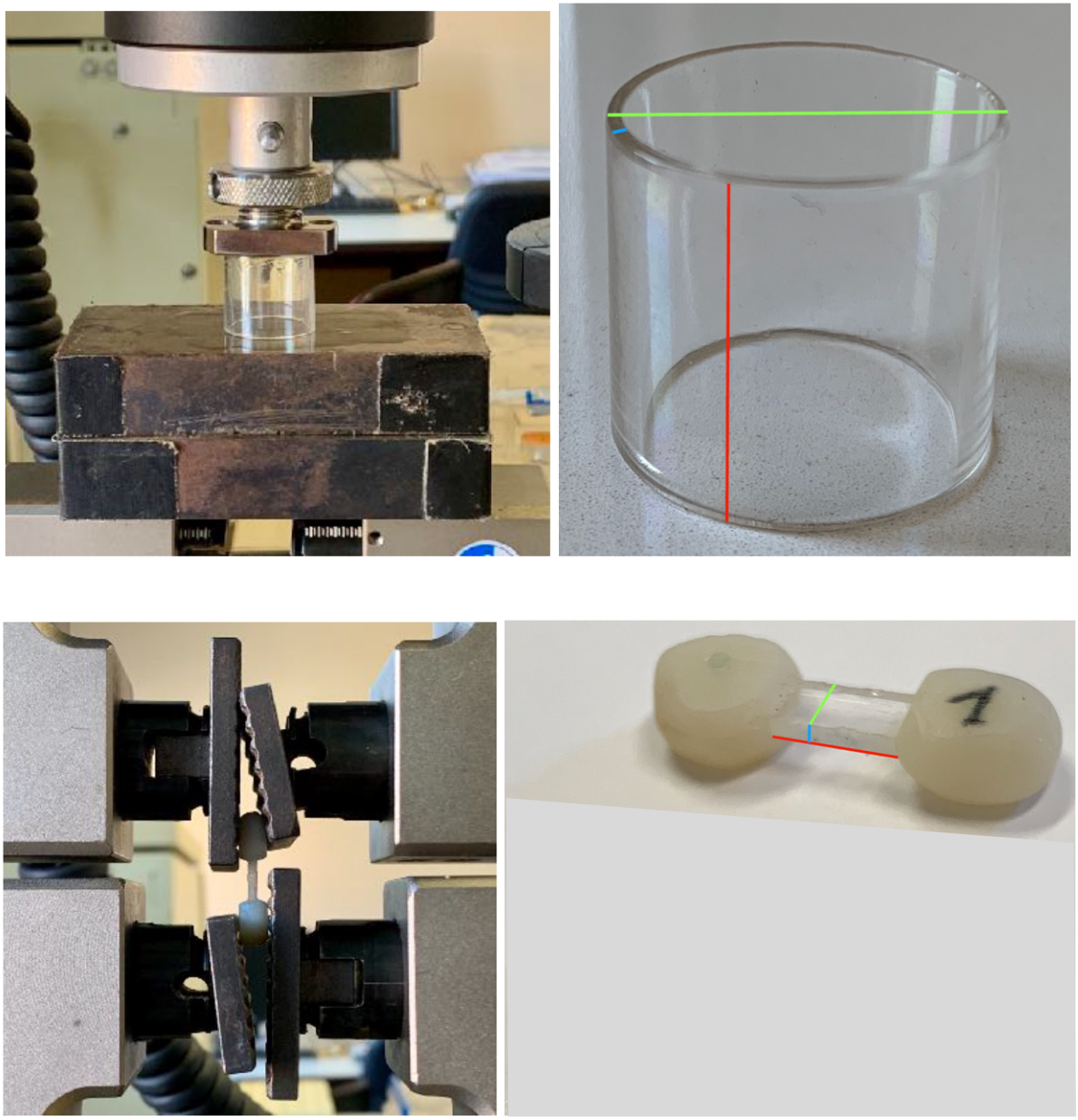

Figure 11: Material testing of PC. A cylinder-like specimen was tested in compression (sample 1: 20.0 mm height × 1.5 mm thickness × 22.0 mm Ø) (**upper**), and a beam-like specimens was tested in tension (4.0 mm width × 1.5 mm thickness × 7.0 mm length) (**lower**).

For obtaining mechanical data for the FEA, the VMQ was tested in uniaxial tension by locking the terminal parts of the specimen in SS clamps. Two specimens were used, one representing thinner parts (2.5 mm width × 3.5 mm thickness × 24.0 mm length), and one representing thicker parts (4.5 mm width × 4.5 mm thickness × 24.0 mm length), which consisted of beams of silicone cut from the contour of the nasal surface of the mask. Tests were performed at speed of 2 mm/min, and 4 mm/min, respectively, up to 5 mm of displacement (**Figure 12**).

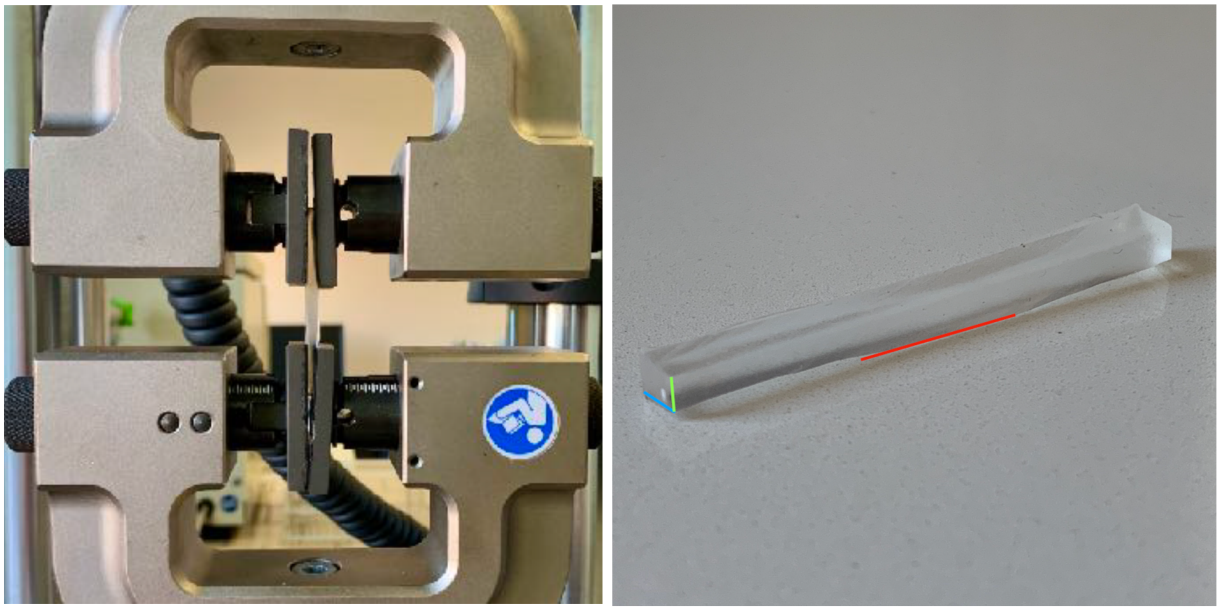

Figure 12: Material testing of silicone. Two string-like specimens were tested in tension (sample for thinner parts: 2.5 mm width × 3.5 mm thickness × 24.0 mm length; sample for thicker parts: 4.5 mm width × 4.5 mm thickness × 24.0 mm length).

For obtaining mechanical data for the FEA, the headgear bands material was tested in uniaxial tension by locking the terminal parts of each specimen in SS clamps. Two specimens were used, one representing shorter parts (20.0 mm width × 2.5 mm thickness × 55.0 mm length), and one representing longer parts (20.0 mm width × 2.5 mm thickness × 194.0 mm length), which consisted of cut parts of the band of the same width. The initial position of the tested specimens with respect to the clamping device was marked with a permanent marker, in order to ensure that no slippage occurred during testing. Tests were performed at 60 mm/min, up to 20 N of force (**Figure 13**).

Figure 13: Material testing of the headgear bands. The structure was tested in tension (sample for shorter parts: 20.0 mm width × 2.5 mm thickness × 55.0 mm length, sample for longer parts: 20.0 mm width × 2.5 mm thickness × 194.0 mm length).

In addition, for the purpose of validating the FEA model of the forehead support, the complex structure made of a PC frame and a VMQ cushion that constituted it, was tested in uniaxial compression positioning the specimen (PC frame: 28.0 mm width × 5.0 mm thickness × 80.0 mm length, and silicon cushion: 24.0 mm width × 20.0 mm thickness × 64.0 mm length) on a SS flat plate and pressed with the head of the machine mounting a SS flat tip (20.0 × 26.0 mm). Test was performed starting without contact on the surface of the specimen, which consisted of the PC forehead support with VMQ cushion that was separated from the mask by using a high-speed cutting disk. Test was performed at a speed of 2.0 mm/min up to 20 N of force (**Figure 14**).

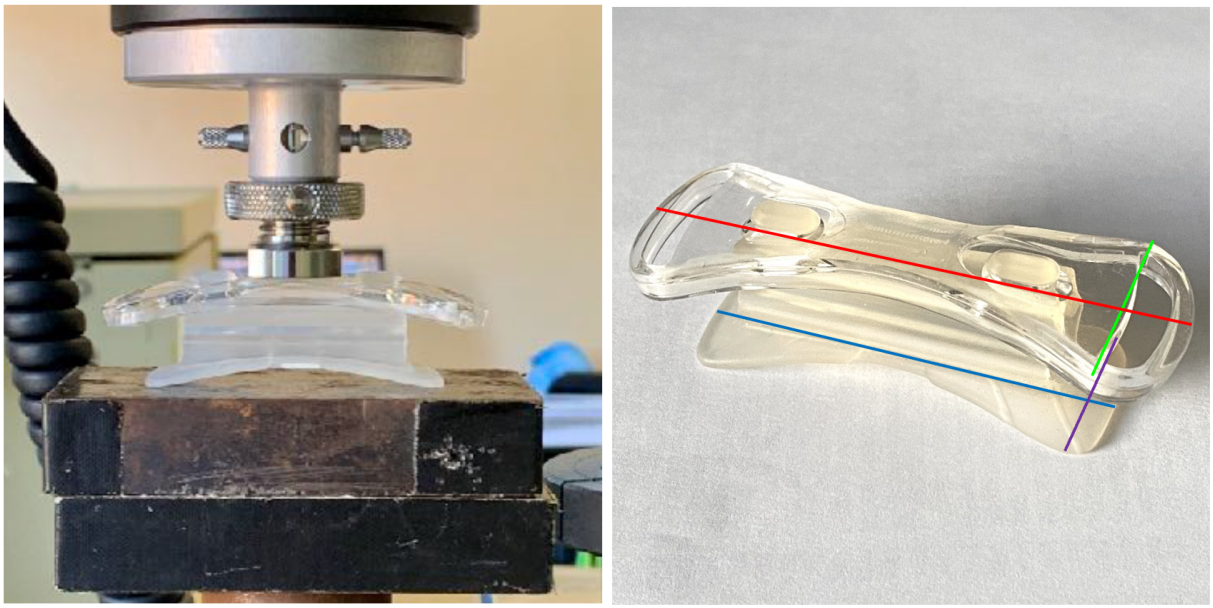

Figure 14: Material testing of the PC and VMQ structure forming the forehead support. The structure was tested in compression (PC frame: 28.0 mm width × 5.0 mm thickness × 80.0 mm length; VMQ cushion: 24.0 mm width × 20.0 mm thickness × 64.0 mm length).

Load (N) vs. displacement (mm) curves were converted into stress (σ) vs. strain (ε) curves, and the Young's modulus (E) was calculated.

Strain (ε, mm/mm) was calculated as:

$$\varepsilon = ½ \{[(l_0 + u) / l_0]^2 - 1)\}$$

Where l_0 (mm) was the initial length, and u (mm) was the incremental displacement.

Stress (σ, N/m^2 or Pa) was calculated as:

$$\sigma = F / A_C = F / [A_0 \times (1 - \varepsilon/2)^2]$$

Where F (N) was the force, A_C (m^2) the contact area, and A_0 (m^2) the initial contact area.

And Young's modulus (E) was calculated as:

$$E = \sigma / \varepsilon$$

So they could be used in the FEA model.

2.5 Application and registration of the position of the pressure-mapping sensors

Four commercial resistive-type pressure-mapping sensors with trimmable configuration (model 4201, 0.1 mm thickness, 45.7 × 21.1 mm matrix, 34 kPa maximum pressure setting, -40° to +60°C temperature range, 1.9 mm pitch, 27.6 sensels/cm^2 resolution, Tekscan, MA, USA) were applied on the phantom head for measuring contact pressures (**Figure 15**).

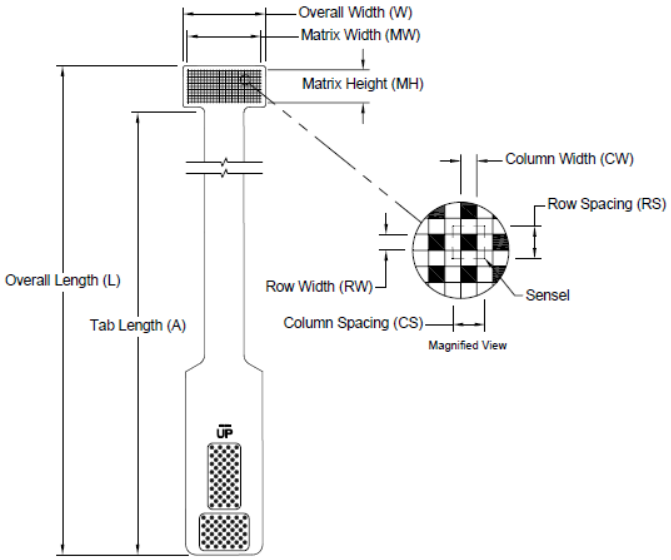

Overall Length	430.8 mm
Overall Width	50.8 mm
Tab Length	402.3 mm
Matrix Height	21.1 mm
Matrix Width	45.7 mm
Thickness	0.178 mm
Row Width	1.0 mm
Row Spacing	1.9 mm
Row Quantity	11
Column Width	1.0 mm
Column Spacing	1.9 mm
Column Quantity	24
Number of Sensing Elements	264
Sensel Density	27.6 sensels/cm^2
Pitch	1.905 mm
Temperature Range (Low//High)	-40 °C // 60 °C
Max Pressure Ranges	34 kPa // 13790 kPa

Figure 15: Characteristics of pressure mapping sensors (Model 4201).

One sensor was applied on the forehead, one on the side of the nasal bridge, one on the zygomatic area, and one on the maxilla. Assuming a symmetrical distribution of forces applied by the mask relatively to the facial midline, sensors were positioned in order to cover the relevant areas only on one side (as results could be mirrored on the opposite side). Sensors had dedicated real-time contact pressure mapping commercial software (I-Scan System, Tekscan, MA, USA) (**Figure 16**).

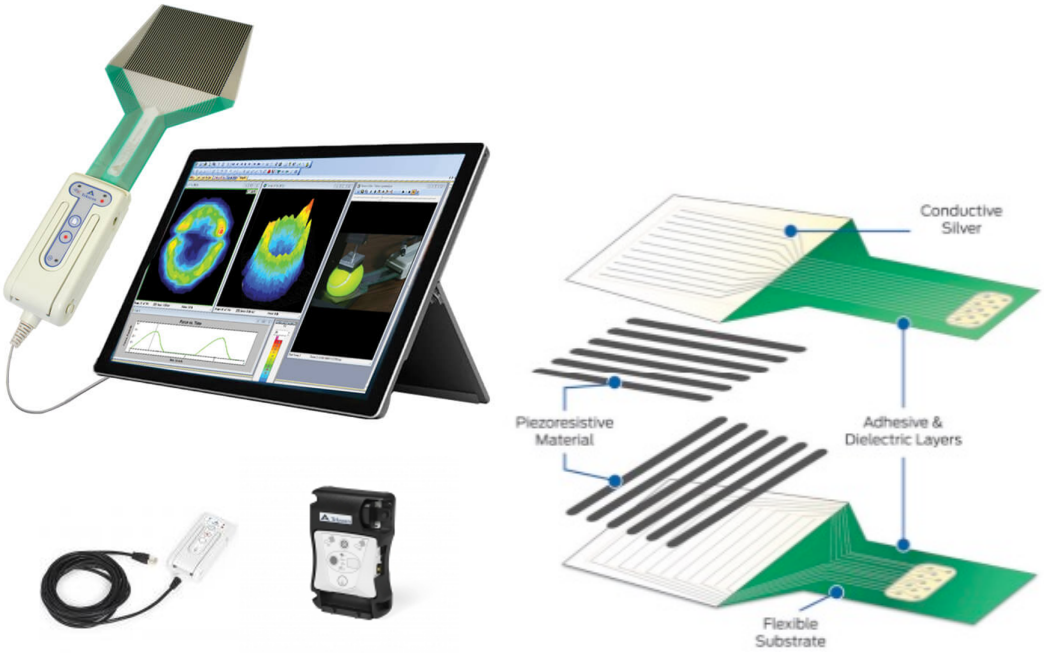

Figure 16: Example of configuration of the real-time contact pressure mapping system (I-Scan, Tekscan) connected to a standard portable computer (**upper**). Handle (VersaTek Handle, Tekscan) on the left, and wired/wireless unit (VersaTek Unit, Tekscan) on the right (**lower**).

Sensors position was registered through a commercial opto-electronic system (Smart-DX 400, BTS Bioengineering) constituted by 10 digital cameras equipped with infra-red illuminators and optical filters (to reduce optical interferences), and reflective spherical passive markers. Preliminary to acquisition, a static calibration was performed by using a structure equipped with optical markers and representing the cartesian triplet of 3D references. The dynamic calibration of intrinsic and extrinsic system parameters was performed by moving a stick (wand) with markers in the 3D working space (**Figure 17**).

Figure 17: Digital camera, spherical passive markers, structure with reference triplet used for static calibration, and wand used for dynamic calibration. All were components of the commercial system (SMART-DX 400).

Seven markers were attached to the head, creating a 3D reference system for the segment. A probe pointer (constituted by four markers and calibrated by pivoting) was used to scan the facial surface and the 3D position of each sensor with respect to the segment (**Figure 18**).

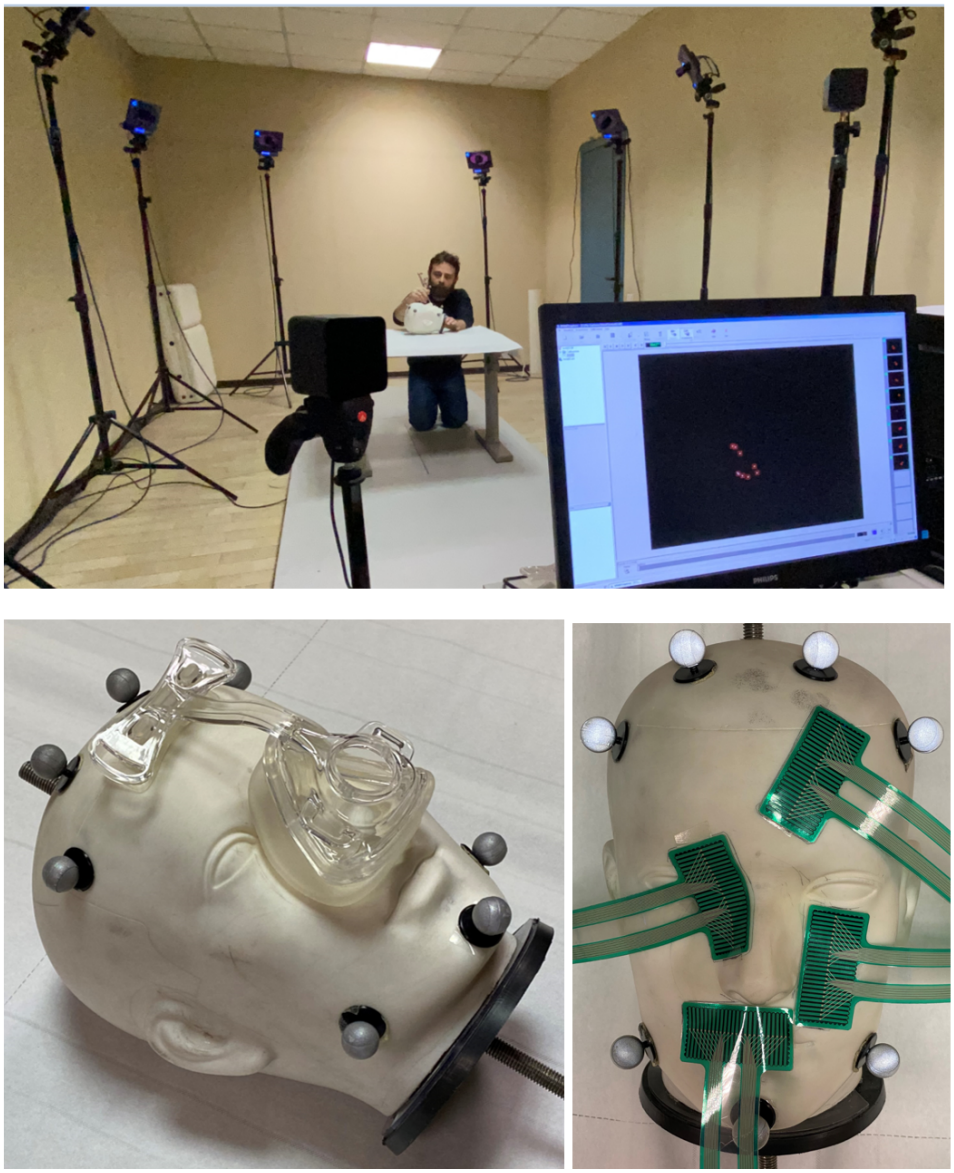

Figure 18: Acquisition of the 3D position of the sensors on the phantom head with reflective markers applied.

Information about facial surface, sensors surface (as they deformed to adhere to the facial surface), and sensors position were acquired as point-cloud non-structured information. Such information was aligned with the 3D head via a rigid registration procedure (Iterative Closest Point Alignment) using a commercial software (MeshLab, ISTI - CNR Research Center, Italy) (**Figure 19**).

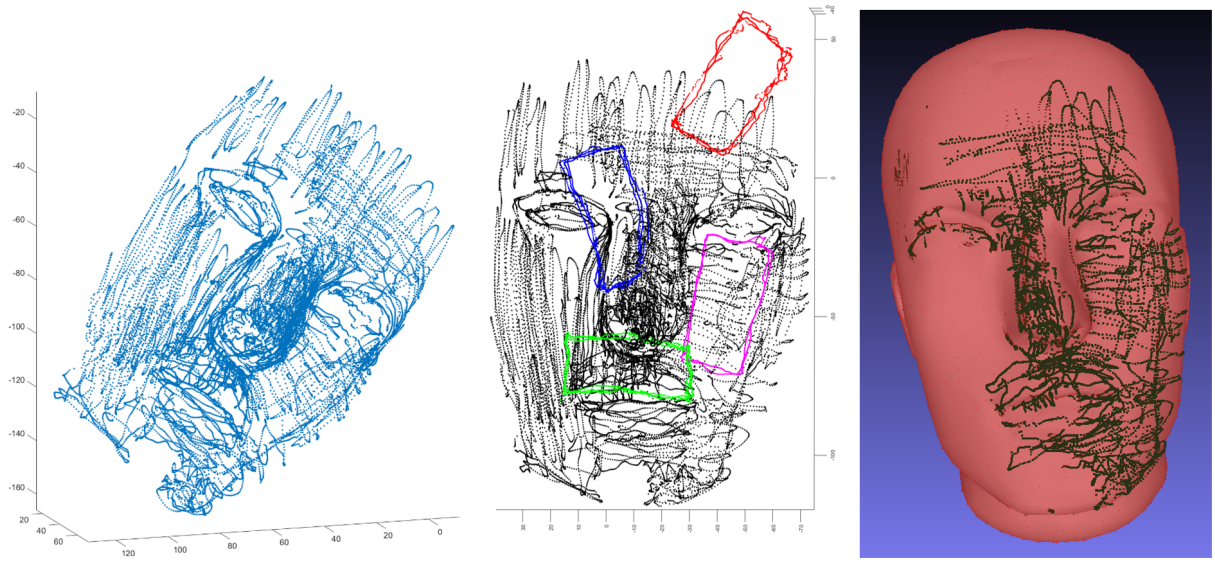

Figure 19: Acquisition of the 3D point-cloud surfaces by optoelectronic system. Detail of the facial surface (**left**) Details of the four contact pressure mapping sensors, each one highlighted in a different colour (**right**).

A mesh model of a sensor was created with commercial software (Blender, Blender Foundation, Netherlands), where each vertex of the 11 × 22 mesh represented a sensible element of the sensor. The mesh was then adapted to the point-cloud acquired for each sensor through morphing tools (Sculping, Blender, Blender Foundation, Netherlands). The recording allowed to transfer the sensors output matrix to the facial surface (accounting for the specific orientation and deformation), for comparison with FEA also in terms of spatial distribution of contact pressure (**Figure 20**).

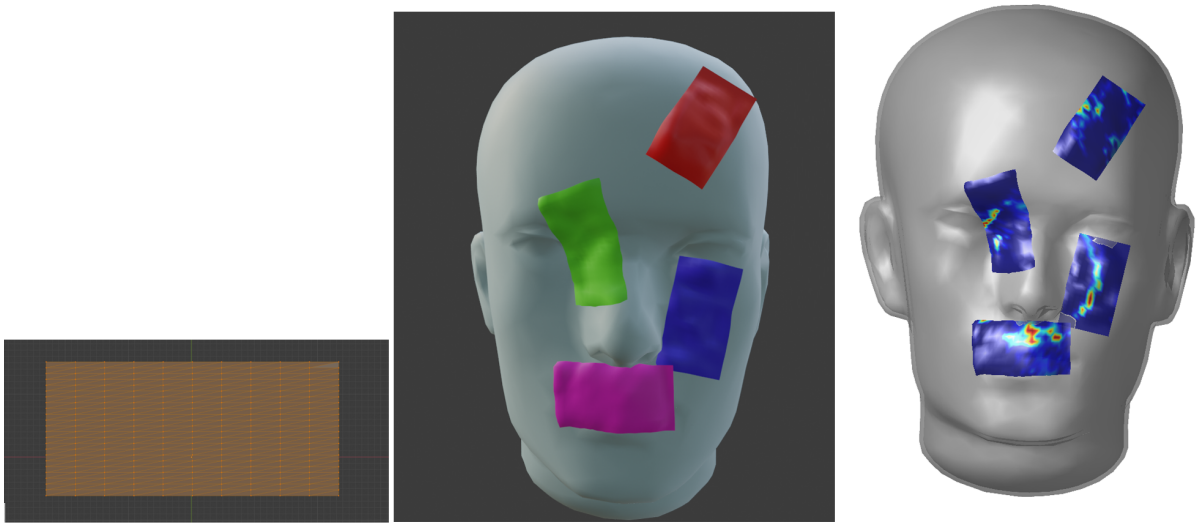

Figure 20: Mesh of a single pressure sensor (**left**). Position of the mesh of each of the four sensors on the 3D model of the head (**centre**). Example of pressure mapping obtained on the four sensors (**right**).

2.6 Calibration of pressure-mapping sensors

Sensors were calibrated before and after data acquisition, using the same mechanical testing machine and settings described above. After application on the head, sensors configuration was set to zero to account for possible deformations due to the irregular facial surface. Then, each sensor was calibrated by stabilising the head so that the surface of the sensor was parallel to the floor (perpendicular to the applied load), and pressure was applied through a flat SS tip (Ø = 14.0 mm) covered with a 2.0 mm silicon layer (**Figure 21**). Sensors were calibrated by linear calibration for single array, with imposed load (5 N, 10 N, 15 N, and 20 N), according to specifications from the manufacturer (Tekscan Linear Calibration, Tekscan, MA, USA).

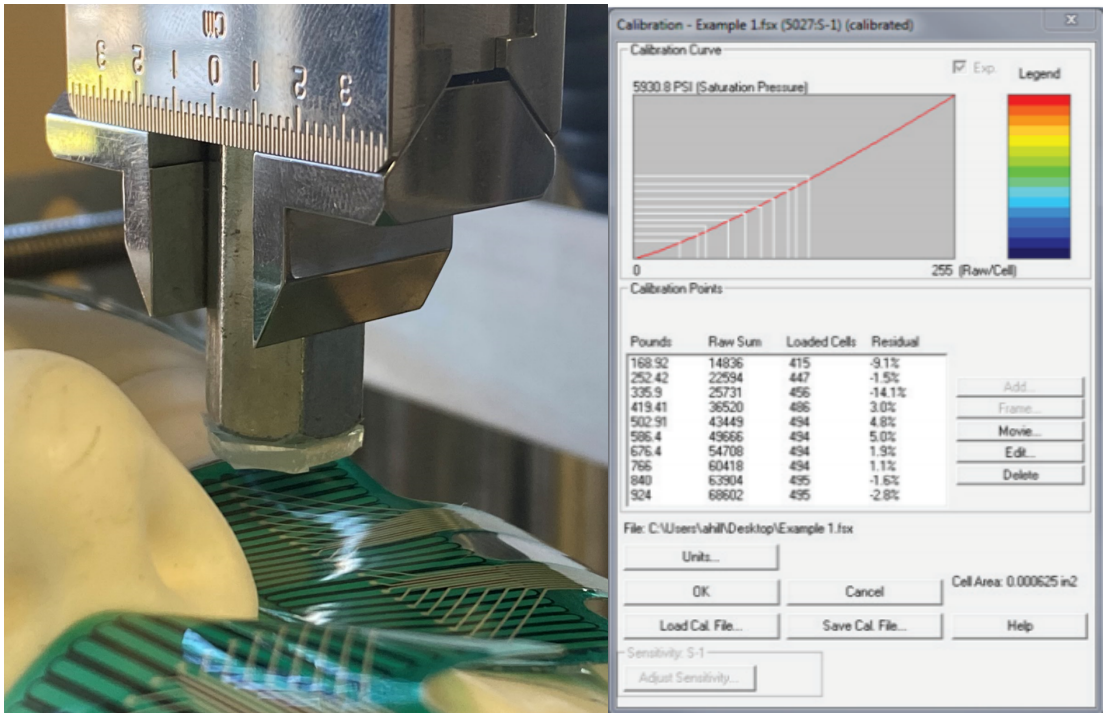

Figure 21: Detail of the calibration of one sensor using the mechanical testing machine.

2.7 Laboratory simulation with direct perpendicular forces

A first series of tests was performed by applying direct perpendicular forces, using a metal sphere as connection between the CPAP mask and the testing machine. These settings were adopted in order to have a simplified model with simpler and controlled load, compared to the clinical application that consists of indirect loading through the headgear bands. Such controlled settings were used for validation of the FEA simulation of the mask.

Tests were performed using the same mechanical testing machine and settings described above. The head was positioned face-up with its main axis perpendicular to the floor and the mask on top. The force was applied, using the mechanical testing machine, perpendicularly to the main axis of the head. A SS sphere (Ø = 25.4 mm) was positioned in the anterior hole of the mask (which is clinically used for connecting the pipe to the mask), in order to facilitate the transferring of a purely axial load and uniform stress distribution. Different magnitudes of force were applied (5 N, 10 N, 15 N, and 20 N), with simultaneous mapping of the pressures from the sensors (**Figure 22**).

The graphical output of pressure mapping sensor of each area was compared with the FEA graphical output at 5 N, 10 N, 15 N, and 20 N.

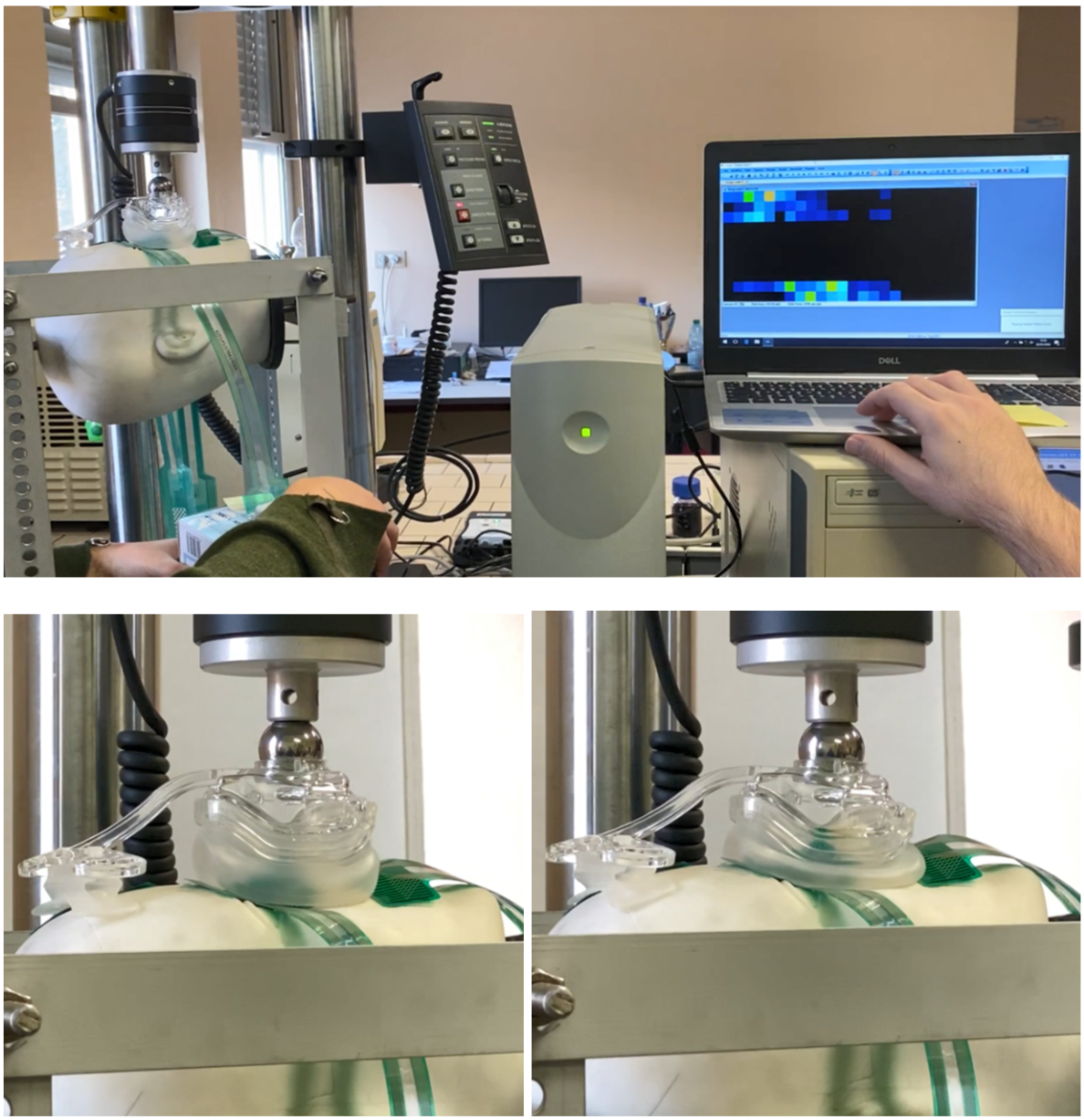

Figure 22: Setup for the mechanical testing with the CPAP directly loaded with the mechanical testing machine.

2.8 Laboratory simulation with indirect forces through the headgear

A second series of tests was performed by applying forces similarly to the clinical application, which implied the use of the headgear. Tests were performed using the same mechanical testing machine and settings described above. The head was positioned face-down with the main axis perpendicular to the floor. The mask was connected to the headgear and tensile force was applied to the headgear perpendicularly to the main axis of the head, leading to compression of the mask on the face. The headgear was connected to the mechanical testing machine by a custom-made device consisting of a horizontal SS rod (220 × 20 × 3 mm), so that the upper and lower bends of the headgear were adjusted with Velcro and uniformly loaded. Different magnitudes of force were applied (5 N, 10 N, 15 N, and 20 N), with simultaneous detection of the contact pressures from the sensors (**Figure 23**).

The graphical output of pressure mapping sensor of each area was compared with the FEA graphical output at 5 N, 10 N, 15 N, and 20 N.

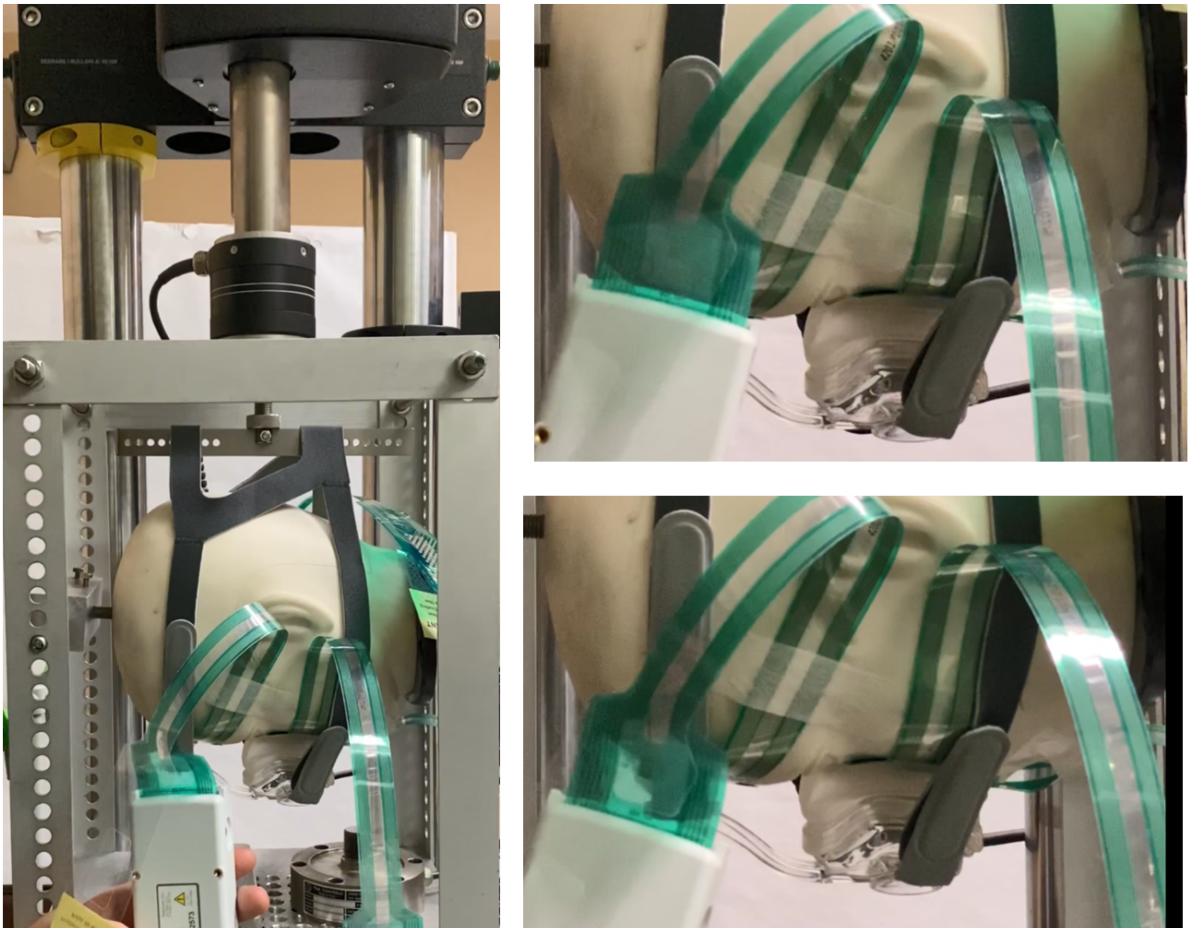

Figure 23: Setup for the mechanical testing with the CPAP loaded with indirect forces through the headgear.

2.9 Finite element analysis of the mask pressures on the face

In solid mechanics, the position of each point (x, y, z) is described as a function (differential equation), and it has infinite variables. In a FEA simulation, the variables are the displacements of each identified point of the FEA model. Thus, a continuous problem with infinite variables is transformed into a discrete problem with a finite number of variables, shifting from differential equations (which calculate functions) to simple equations (which calculate numbers). In particular, the present simulation included a non-linear system of equations. Suitable geometries were acquired as mentioned above (**Figure 24**).

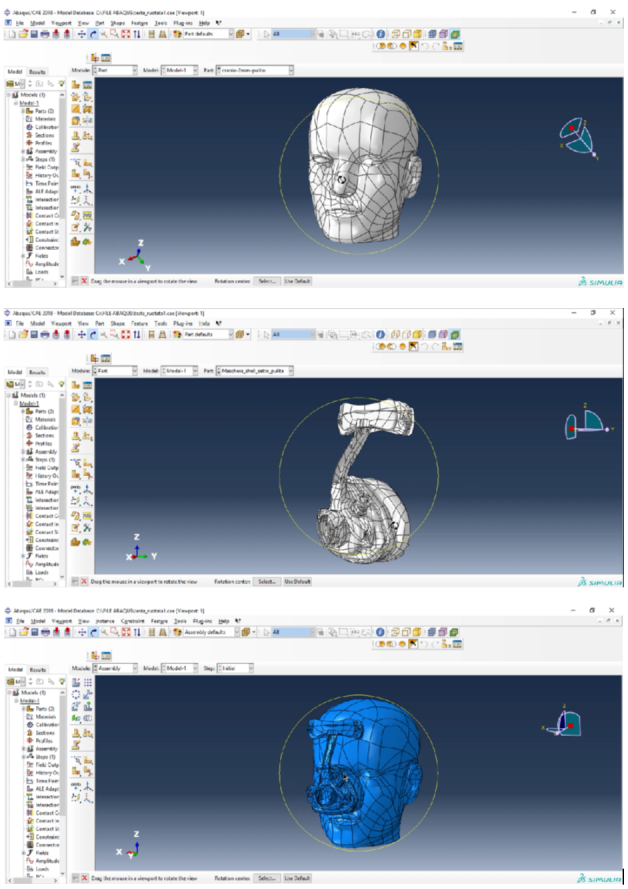

Figure 24: Finite elements analysis (FEA) objects.

Then, software setting were defined such that the geometry was considered as a solid to be loaded (discretisation phase).

Firstly, materials were defined and the head was considered as completely rigid surface not attributable to any specific material (in order to avoid to generate a mal-conditioned system due to the large difference in the Young's modulus between the head and the tested VMQ of the CPAP mask). This assumption was supported by the fact that the maximum applied load (20 N) was unable to generate non-negligible deformation of a PVC phantom head filled with class IV gypsum. The VMQ, instead, was defined as a linear elastic material with a Young's modulus of 1.27 MPa for thin parts and 1.31 MPa for thick parts, according to the results of the mechanical tests. Tests revealed linear force-displacement curves within a deformation range of about 20% (greater deformations that may lead to non-linear behaviour were not considered as they were not relevant to the clinical settings). The Poisson coefficient was defined as 0.4 (from the published literature), for both thin and thick parts (considering that a number closer to 0.5 may create numerical difficulties). A density of 1.2×10^{-9} (N/mm^2) × s^2 was retrieved from a commercial datasheet *(Guarnipol)*. The Young's modulus of the PC constituting the frame of the CPAP mask was measured in the laboratory test as 226 MPa in compression and 1190 MPa in tension, and it was considered as completely rigid for the same assumption adopted for the phantom head.

The neoprene/nylon bands of the headgear were defined as a linear elastic material with a Young's modulus of 1.66 MPa for short bands and 1.38 MPa for long bands, according to the results of the mechanical tests. The Poisson coefficient was defined as 0.45 (from the published literature), for both short and long parts (considering that a number closer to 0.5 may create numerical difficulties). A density of 9.5×10^{-10} (N/mm^2) × s^2 was retrieved from a commercial datasheet *(Guarnipol)*. A frictional coefficient of 0.1 was used for the sliding of the headgear bands on the head.

Thicknesses also had to be defined since the model was simplified to a shell one (and not a 3D one). Only the thicknesses of the VMQ cushion were measured, since the face and the CPAP frame were considered as rigid surfaces. Thicknesses of the VMQ cushion were measured with a calliper and a feeler gauge, and varied between 0.7 and 3.5 mm (unfortunately, shell elements do not allow a gradual thickness reduction, and an intermediate step of 1.5 mm thickness was used). However, thicknesses were later adjusted in order to obtain a more coherent mechanical behaviour with respect to the laboratory test (which were used as reference) (**Figure 25**).

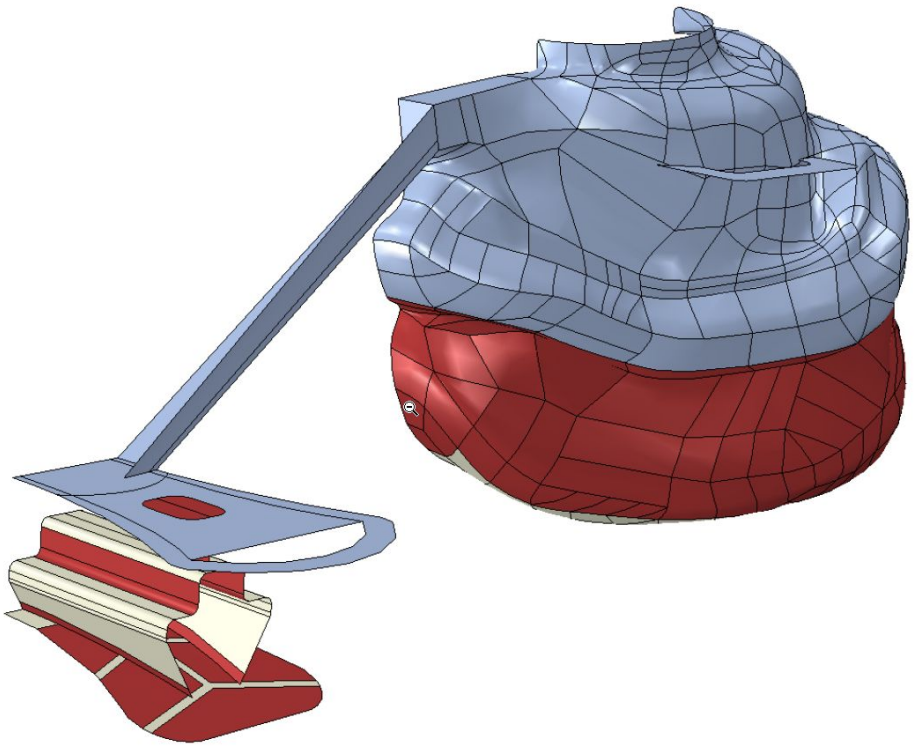

Figure 25: Materials constituting the mask and the different thicknesses are represented with different colours.

Position and orientation of each object had to be defined as well, including the rigid frame of the CPAP mask, the soft VMQ cushion, and the rigid head. For simplicity, it was assumed a condition of symmetry of geometries, constraints, and loads, with respect to the midsagittal plane of the head. This assumption reduced the variables to half, leading to a time of calculation eight times smaller. Regarding the geometry, all parts were aligned with respect to their symmetry on the midsagittal plane. Four initial (pre-loading) angulations on the midsagittal plane (between the main axis of the head and the main axis of the mask, at 1° difference), were tested for each type of loading. Constrains were that the head was immovable (a single constrain on a rigid object), and that movements along the symmetry plane were not allowed (**Figure 26**).

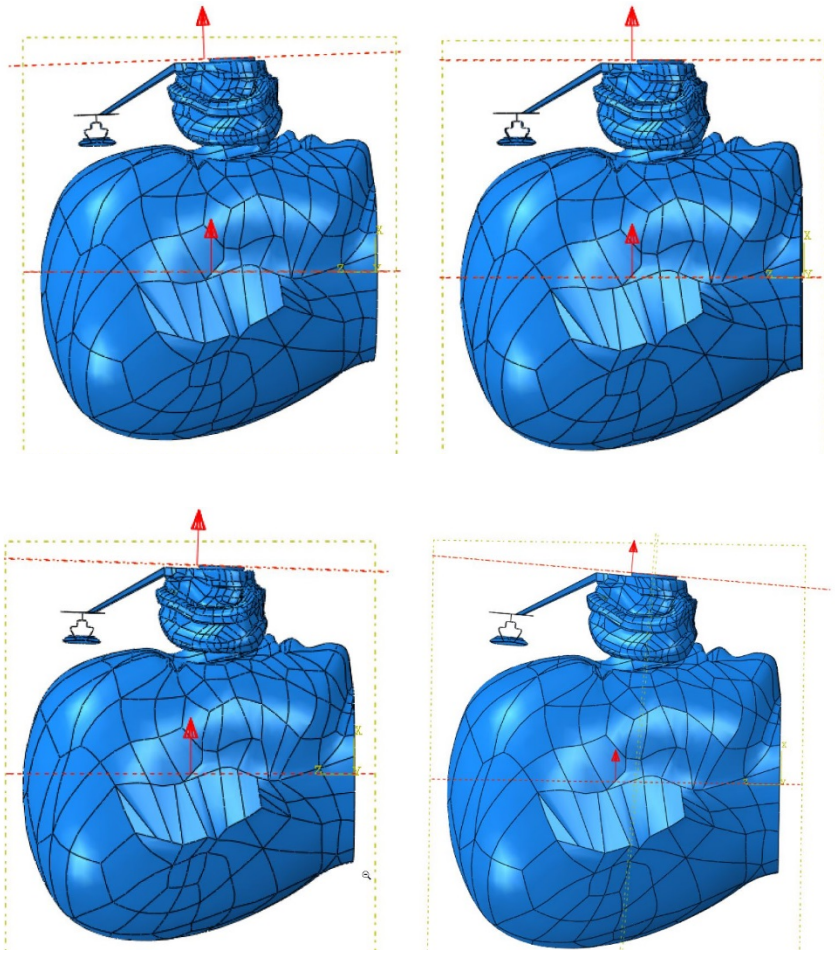

Figure 26: Different initial angulations between mask and head used in the FEA model.

The type of FEA can be based either on fast loading (accounting for inertia forces *i.e.*, dynamic loading) or slow loading (inertia forces are neglected *i.e.*, static or quasi-static loading). Then, either small displacements or big displacements can be considered. In the investigated setting, displacements were big, since the VMQ was assumed to undergo macroscopic deformation under loading. Unfortunately, the two relevant surfaces (head and VMQ) could not be automatically interfaced, and it was necessary to use dynamic loading to make the mask fall on the face because of gravity:

- The weight of (half) CPAP mask (gravity = 9810 mm/s^2 × density of VMQ) was applied to the mask, so that it moved towards the head along an x-axis (passing through the nose), in 1 s;
- The weight of (half) metal sphere (0.5549 N + gravity) was applied to the sphere (which was used for loading the CPAP mask during the experiment with direct perpendicular forces), so it further loaded the CPAP mask along the same x-axis, in 1 s;
- (Half of) the loading generated by the mechanical testing machine (loading = 0.5549 N + 10 N + gravity) was finally applied, in 10 s;

The only interfaces of interest were the one between the mid-face and the peri-nasal cushion, and the one between the forehead and the frontal cushion. Thus, in the FEA, the peri-nasal cushion was considered as firmly attached to the rigid frame (the points contacting the two surfaces move together). Whereas, on the interfaces between the cushions and the face, the two objects could be detached but they could not invade each other's volume (contact condition). This implied the presence of frictional forces in case of sliding, which were treated according to the Coulomb model (**Figure 27**).

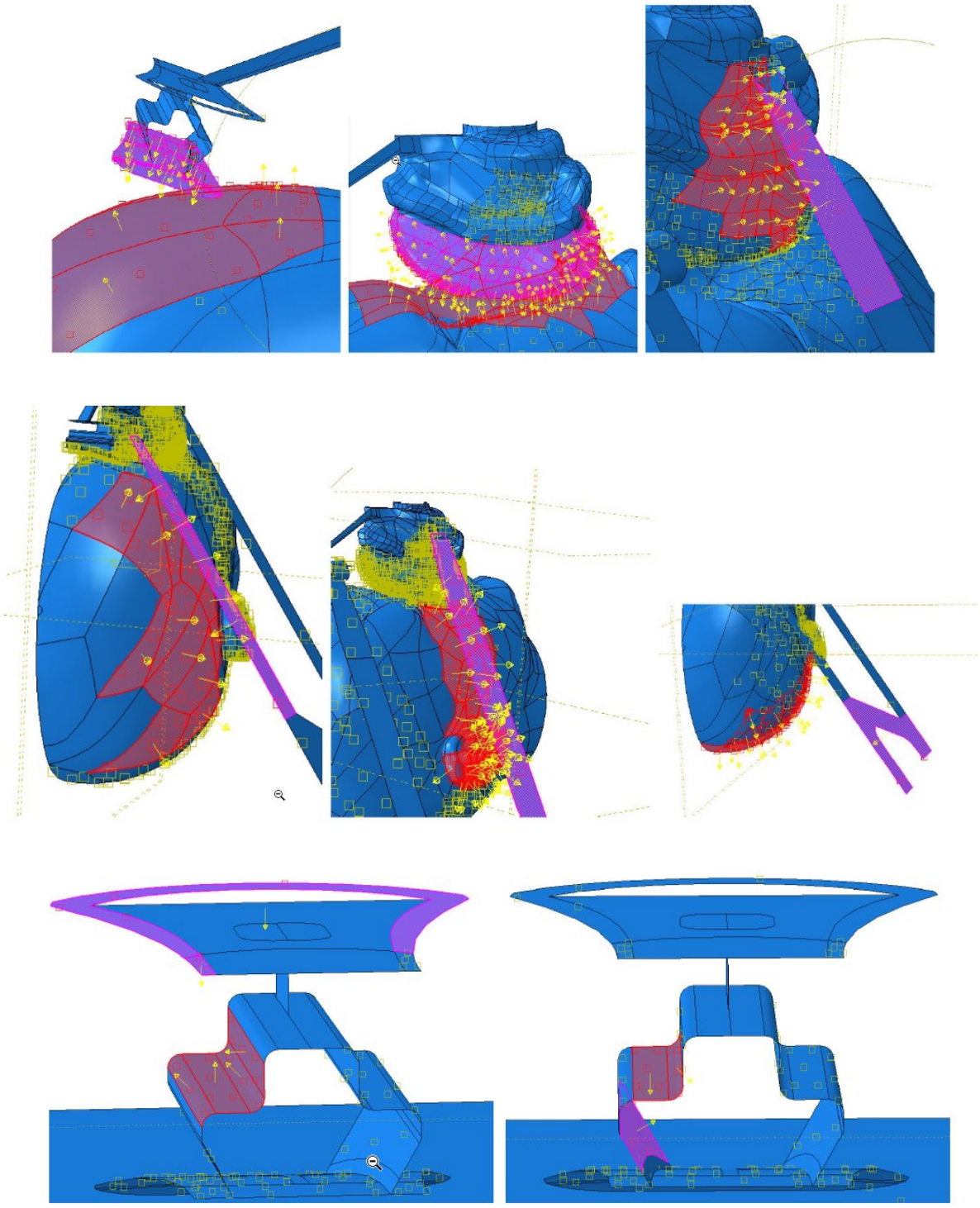

Figure 27: Contact interaction and loading between the surfaces as set in the FEA model.

Then, the mesh was set deciding the number of nodes (their density in specific areas, based on the clinical interest), and the geometry of the finite elements that connect the nodes. In particular, generic shell-type finite elements with triangular shape, with 3 nodes, linear, and accounting for big deformations (bending and stretching) were adopted (S3 type).

Lastly, the analysis was launched by using simulation software (Abaqus/CAE, Dassault Systèmes, 2015, Simulia), with application of forces up to 20 N. The analysis was carried by using a workstation with two 8-core physical processors (each with 8 sub-processors in parallel), which lasted for about 1.5 hours. The outcome variables were the maximum pressure (kPa), the average pressure (kPa), and the area (mm^2), for each analysed region (frontal, zygomatic, nasal, and maxilla). Distributions of forces were calculated and graphically illustrated via a colour scale (from blue to red).

3. RESULTS

Firstly, the mechanical properties of the mask materials were analysed by plotting the data obtained during the mechanical testing of the specimens sectioned from it. Then, the FEA was described, which included the data obtained by the characterisation of the materials. The results of the laboratory test were also described and compared with the data from the FEA.

3.1 Mechanical properties of CPAP mask materials

The PC under compression showed a linear force/displacement (N/mm) relationship ($R^2 = 1.00$, $y = 1095x + 0.54$) from 0 to 20 N.

The PC under tension showed a linear force/displacement (N/mm) relationship ($R^2 = 1.00$, $y = 1022x + 0.30$) from 0 to 20 N (**Figure 28**).

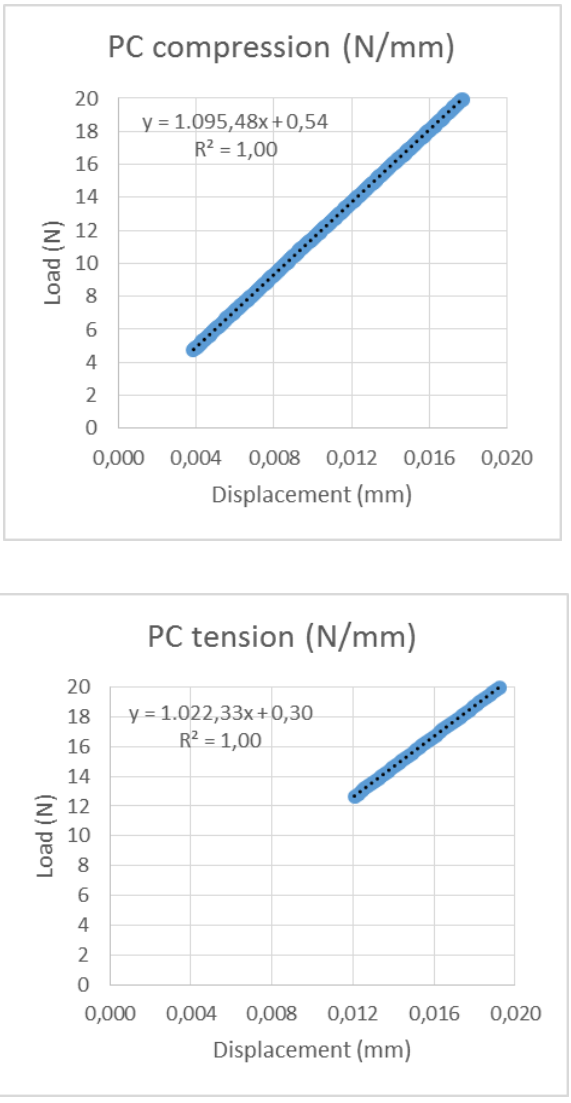

Figure 28: Force-displacement mechanical characterisation of PC under compression (**upper**) and under tension (**lower**).

The PC under compression showed a linear stress/strain (σ/ε) relationship ($R^2 = 1.00$, $y = 226{,}675{,}943x + 5{,}664$) from 0 to 20 N, with Young's modulus of 226 MPa.

The PC under tension showed a linear stress/strain (σ/ε) relationship ($R^2 = 1.00$, $y = 1{,}190{,}041{,}175x + 53{,}475$) from 0 to 20 N, with Young's modulus of 1,190 MPa. (**Figure 29**).

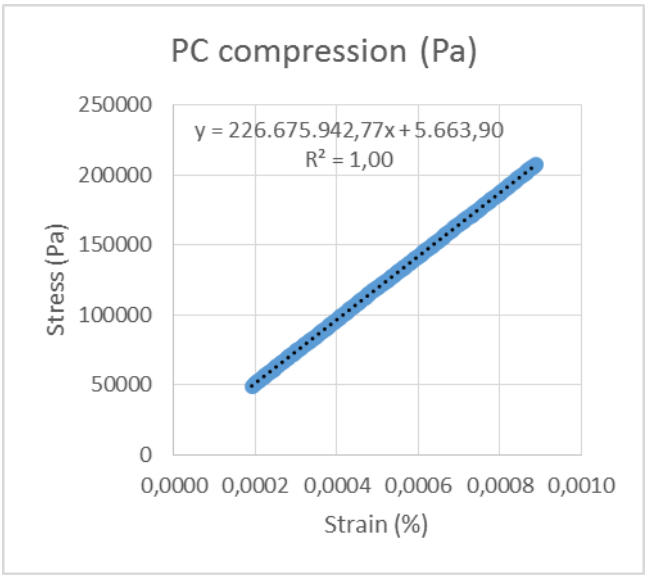

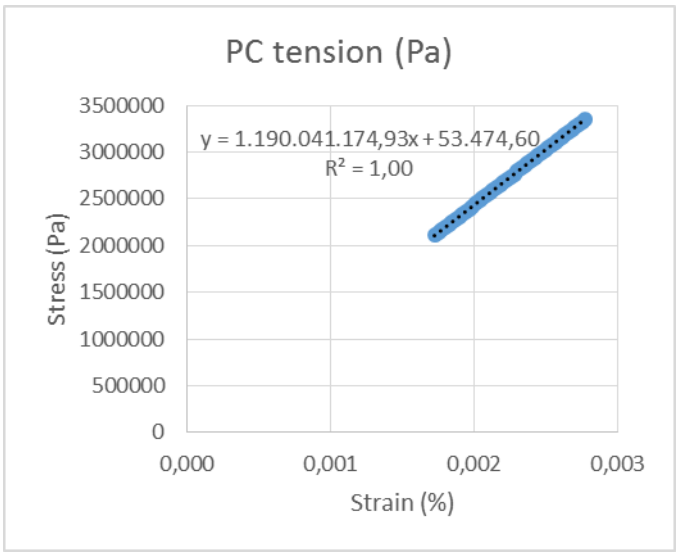

Figure 29: Stress-strain mechanical characterisation of PC under compression (**upper**) and under tension (**lower**).

The thin specimen of VMQ under tension showed a linear force/displacement (N/mm) relationship ($R^2 = 1.00$, $y = 0.51x - 0.04$) from 0 to 5 mm.

The thick specimen of VMQ under tension showed a linear force/displacement (N/mm) relationship ($R^2 = 1.00$, $y = 1.21x – 0.27$) from 0 to 5 mm (**Figure 30**).

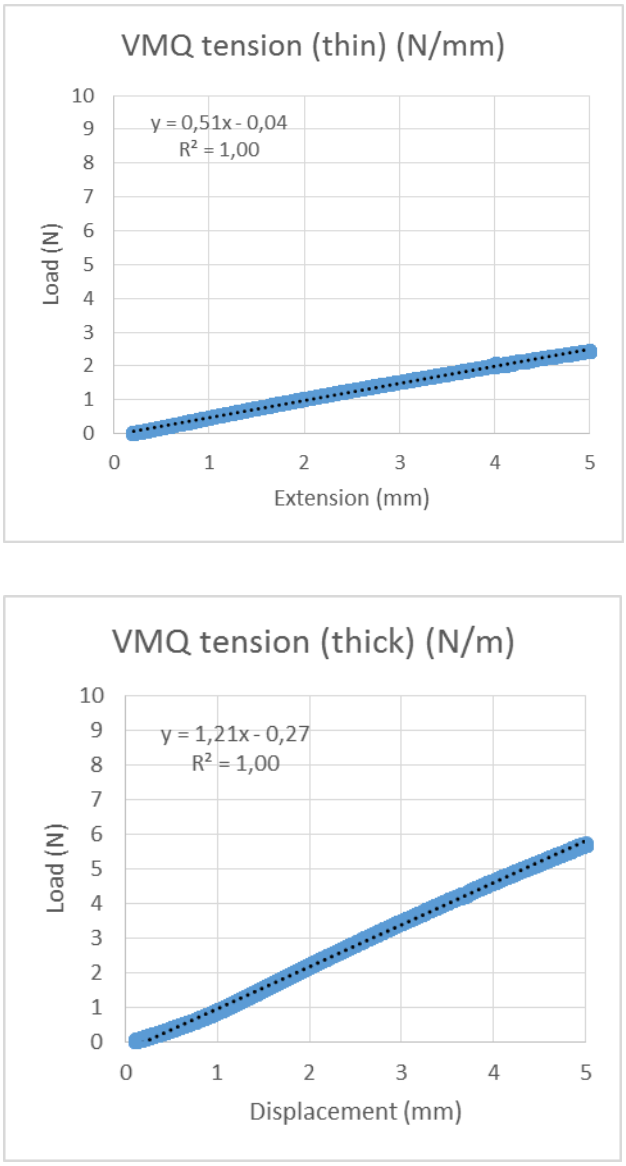

Figure 30: Force-displacement mechanical characterisation of VMQ under tension, with specimens representing thinner parts (**upper**) and thicker parts (**lower**).

The thin specimen of VMQ under tension showed a linear stress/strain (σ/ε) relationship ($R^2 = 1.00$, $y = 1{,}269{,}287x + 271$) from 0 to 5 mm, with Young's modulus of 1.27 MPa.

The thick specimen of VMQ under tension showed a linear stress/strain (σ/ε) relationship ($R^2 = 1.00$, $y = 1{,}314{,}799x - 8{,}985$) from 0 to 5 mm, with Young's modulus of 1.31 MPa (**Figure 31**).

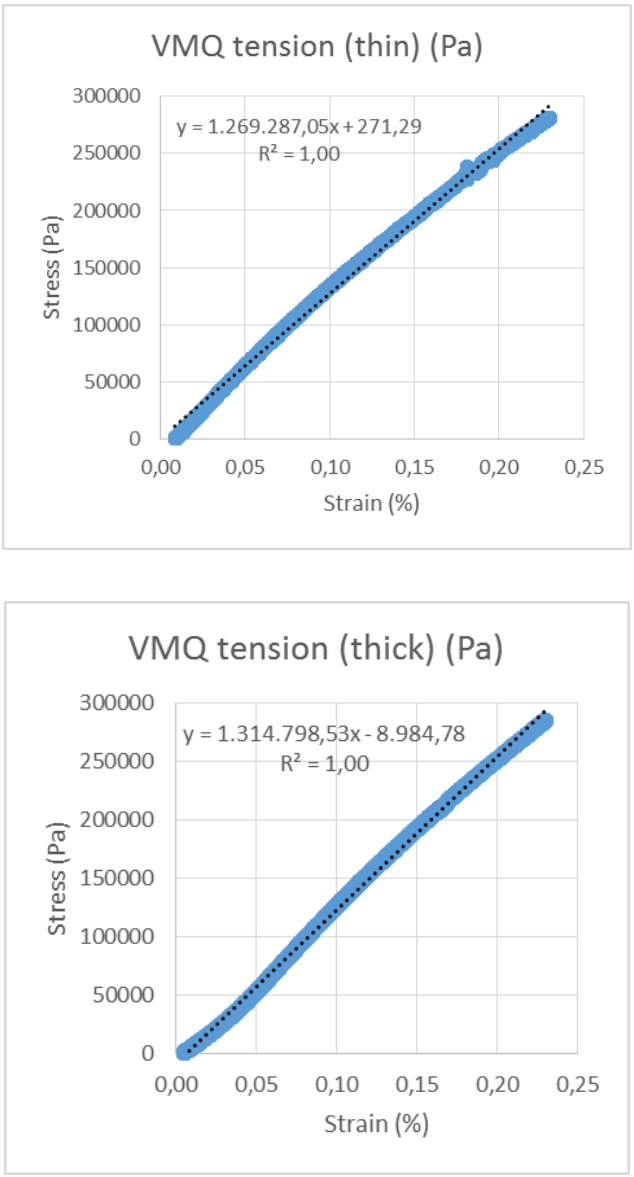

Figure 31: Stress-strain mechanical characterisation of VMQ under tension, with specimens representing thinner parts (**upper**) and thicker parts (**lower**).

The composite structure of PC and VQM under compression showed an exponential force/displacement (N/mm) relationship ($R^2 = 0.96$, $y = 0.13e^{0.55x}$) from 0 to 20 N (**Figure 32**). This was not used for mechanical characterisation, and it was used for the validation of the FEA model instead. The non-linear relationship can be explained by the fact that the VMQ undergoes progressive compression until a transition from the low-modulus VMQ to the high-modulus PC happens.

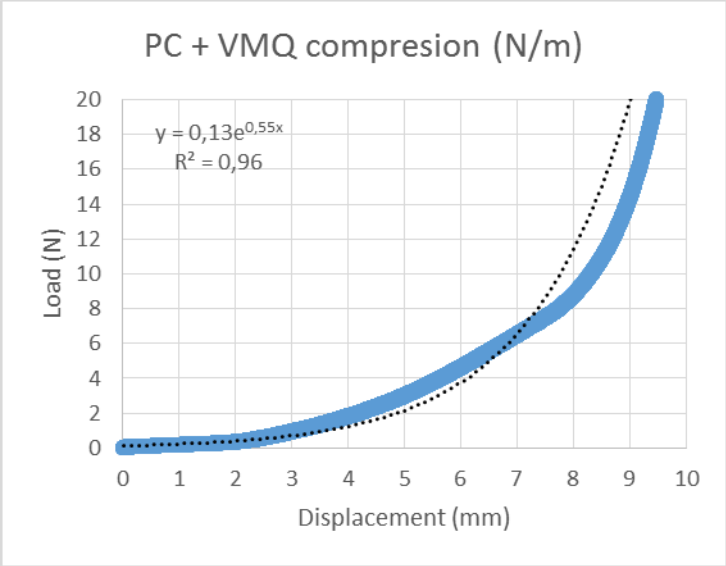

Figure 32: Force-displacement mechanical characterisation of PC and VMQ structure forming the forehead support.

The short neoprene/nylon bend of the headgear under tension showed a linear force/displacement (N/mm) relationship ($R^2 = 0.99$, $y = 1.66x - 1.17$) from 0 to 20 N.

The long neoprene/nylon bend of the headgear under tension showed a linear force/displacement (N/mm) relationship ($R^2 = 0.98$, $y = 0.39x - 1.57$) from 0 to 20 N (**Figure 33**).

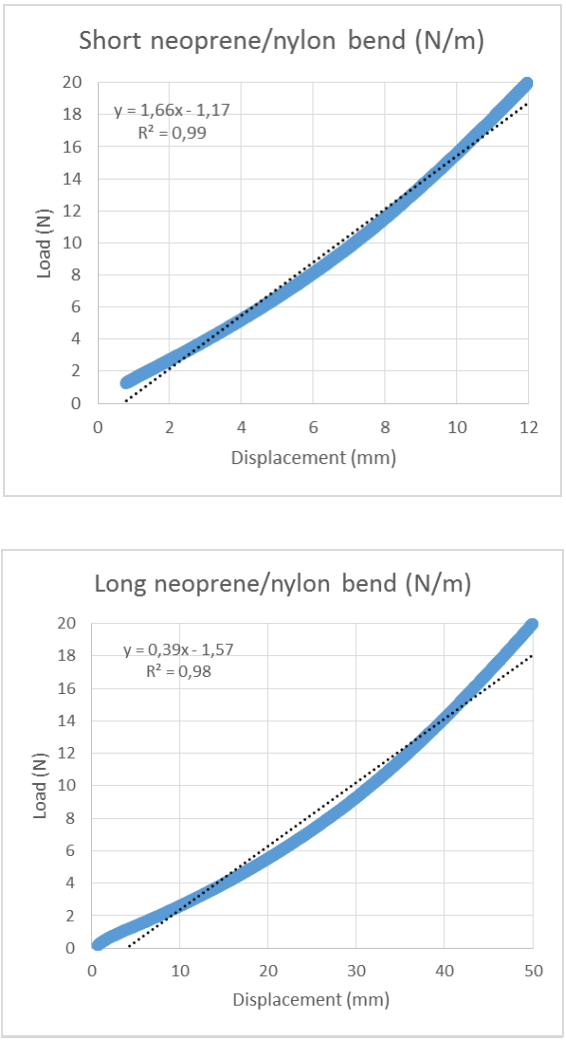

Figure 33: Force-displacement mechanical characterisation of the neoprene/nylon material constituting the headgear bands under tension, with specimens representing short parts (**upper**) and long parts (**lower**).

The short neoprene/nylon bend of the headgear under tension showed a linear stress/strain (σ/ε) relationship (R^2 = 0.99, $y = 1{,}658{,}773x - 16{,}971$) from 0 to 20 N, with Young's modulus of 1.66 MPa.

The long neoprene/nylon bend of the headgear under tension showed a linear stress/strain (σ/ε) relationship (R^2 = 0.98, $y = 1{,}378{,}227x - 25{,}947$) from 0 to 20 N, with Young's modulus of 1.38 MPa (**Figure 34**).

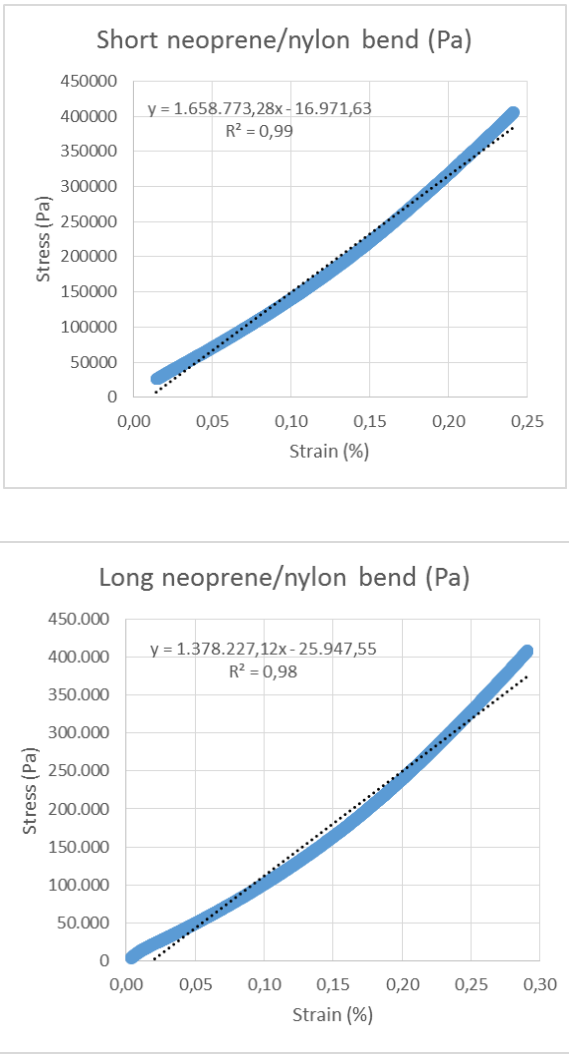

Figure 34: Stress-strain mechanical characterisation of the neoprene/nylon material constituting the headgear bands under tension, with specimens representing short parts (**upper**) and long parts (**lower**).

3.2 Laboratory simulation with perpendicular forces

When direct perpendicular forces were applied, the forehead area did not show relevant variations in maximum (about 12 kPa) or average (about 6 kPa) contact pressure, when force increased from 5 to 20 N. However, the contact area increased from 44 to 149 mm^2 (+238%). This was the area where the smallest contact pressure and areas were detected.

The zygomatic area also did not show great variations in maximum (about 71 kPa) or average (about 23 kPa) pressure, when force increased from 5 to 20 N. However, the contact area increased from 105 to 192 mm^2 (+82%). This was the area where the highest contact pressures were detected.

The nasal bridge area also did not show great variations in maximum (about 25 kPa) or average (about 11 kPa) pressure, when force increased from 5 to 20 N. However, the contact area increased from 58 to 152 mm^2 (+162%). In this area the detected contact pressure were intermediate.

The maxillary area showed an increase in maximum (from 20 to 63 kPa) and average (from 8 to 17 kPa) pressure, when force increased from 5 to 20 N. In addition, the contact area increased from 196 to 431 mm^2 (+119%). This was the area where the highest contact areas were detected (**Table 1**, **Figure 35** and **Figure 36**).

Direct perpendicular force

		Maximum pressure kPa				Average pressure kPa				Area mm^2			
Applied force		5 N	10 N	15 N	20 N	5 N	10 N	15 N	20 N	5 N	10 N	15 N	20 N
Detected value	Forehead	12,0	12,0	12,0	11,0	6,8	6,8	5,9	5,4	43,5	54,4	101,6	148,8
	Zygoma	69,0	69,0	69,0	80,0	22,8	19,2	27,5	25,5	105,2	163,3	105,2	192,3
	Nasal bridge	23,0	26,0	26,0	26,0	11,2	13,1	10,1	9,8	58,1	65,3	101,6	152,4
	Maxilla	20,0	23,0	23,0	63,0	7,6	7,3	8,5	16,8	196,0	145,2	170,6	431,9

Table 1: Pressure and area values detected in each area when direct perpendicular force was applied.

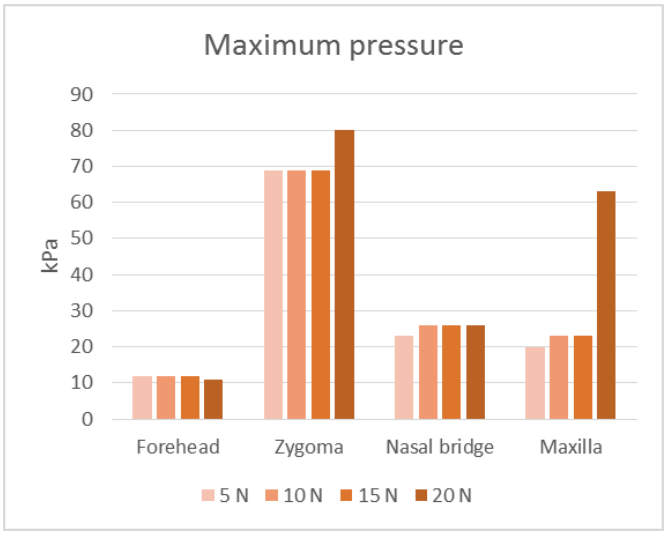

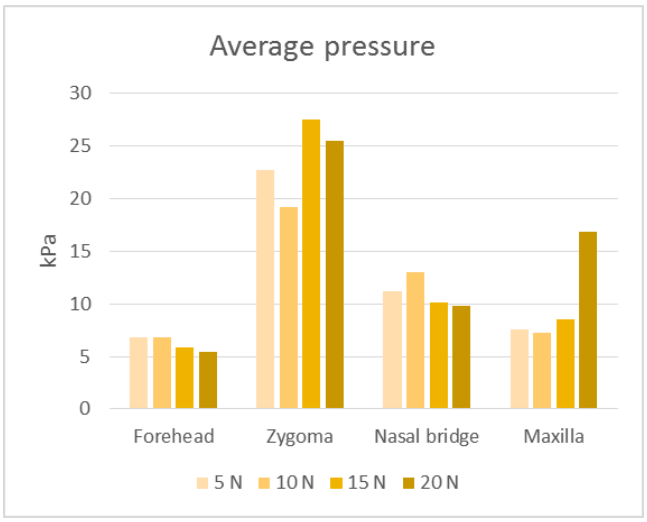

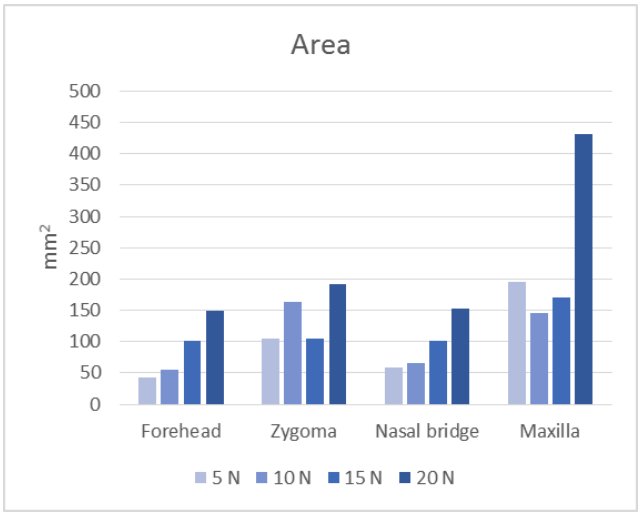

Figure 35: Maximum contact pressure, average contact pressure, and contact area for each analysed region, when direct perpendicular force was applied.

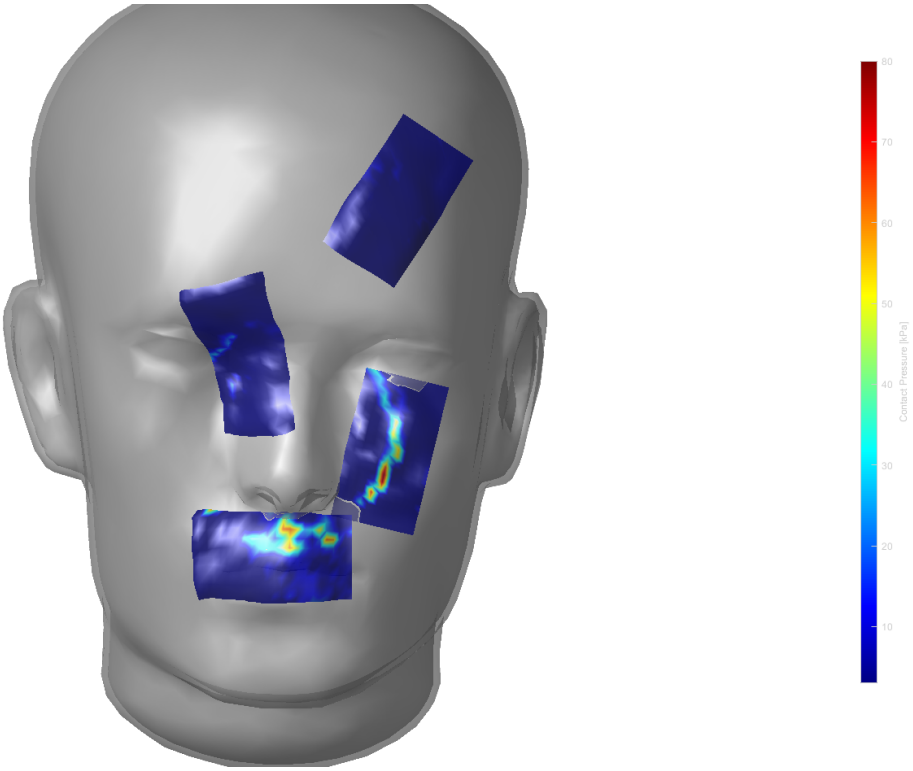

Figure 36: Pressure distributions in the case of direct load configuration.

3.3 Laboratory simulation with headgear forces

When indirect force was applied through the headgear, the forehead area did not show relevant variations in maximum (about 54 kPa) or average (about 13 kPa) contact pressure, when force increased from 5 to 20 N. Similarly, the contact area did not show great variation (about 261 mm^2). Contact pressures and area had intermediate values.

The zygomatic area did not relevant variations in maximum (about 69 kPa) or average (about 20 kPa) pressure, when force increased from 5 to 20 N. Similarly, the contact area did not show great variation (about 138 mm^2). This was the area where the highest contact pressures were detected.

The nasal bridge area did not show relevant variations in maximum (about 23 kPa) or average (about 8 kPa) pressure, when force increased from 5 to 20 N. Similarly, the contact area did not show great variation (about 135 mm^2). This is the area where the lowest contact pressure were detected, together with the maxillary area.

The maxillary area did not show relevant variations in maximum (about 23 kPa) or average (about 8 kPa) pressure, when force increased from 5 to 20 N. Similarly, the contact area did not show great variation (about 321 mm^2). This is the area where the lowest contact pressure were detected, together with the nasal bridge area, but where the highest contact areas were detected (**Table 2**, **Figure 37** and **Figure 38**).

Indirect force through headgear

		Maximum pressure kPa				Average pressure kPa				Area mm^2			
Applied force		5 N	10 N	15 N	20 N	5 N	10 N	15 N	20 N	5 N	10 N	15 N	20 N
Detected value	Forehead	55,0	55,0	52,0	55,0	13,7	13,2	12,1	14,3	261,3	319,4	225,0	239,5
	Zygoma	69,0	69,0	69,0	69,0	18,2	22,0	21,8	19,5	137,9	130,6	137,9	148,8
	Nasal bridge	22,0	23,0	23,0	23,0	7,5	7,3	7,8	9,2	156,0	152,4	108,9	127,0
	Maxilla	23,0	23,0	23,0	23,0	8,1	7,8	7,7	9,7	388,3	315,7	228,6	355,6

Table 2: Pressure and area values detected in each area when indirect force was applied through the headgear.

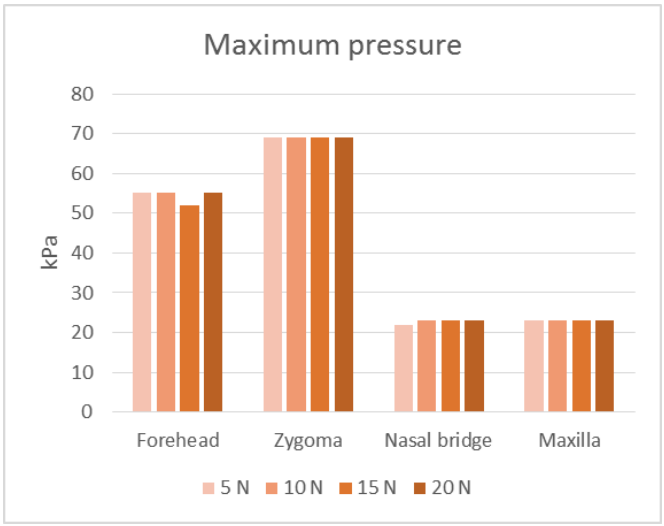

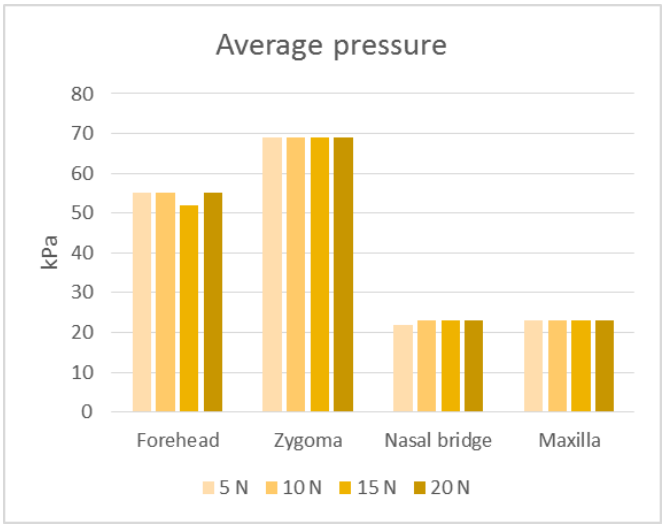

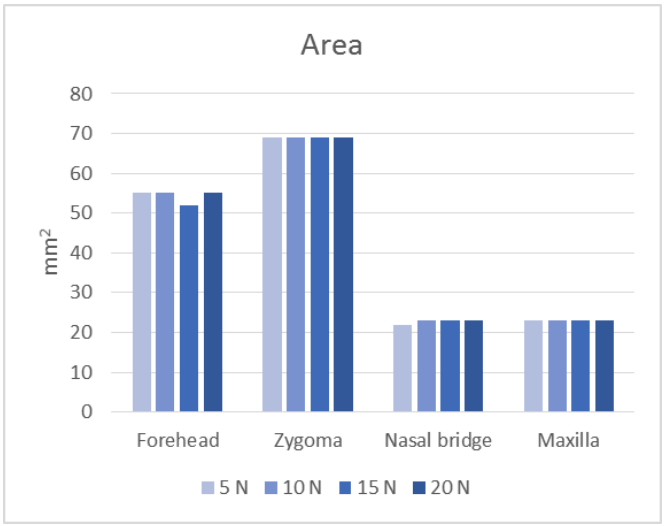

Figure 37: Maximum contact pressure, average contact pressure, and contact area for each analysed region, when direct perpendicular force was applied.

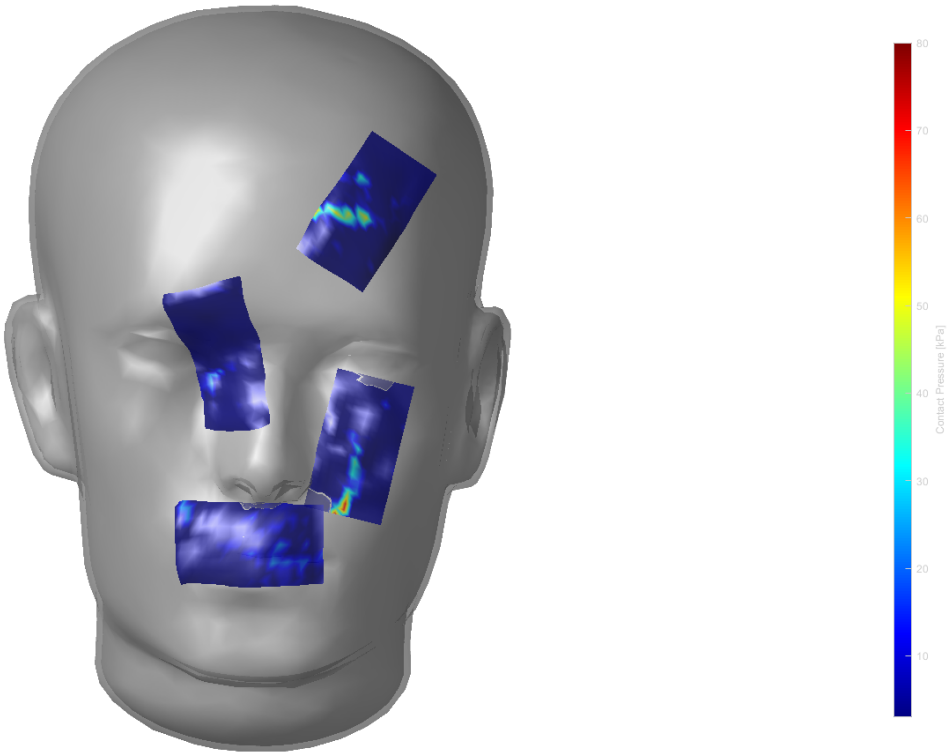

Figure 38: Pressure distributions in the case of load configuration by means indirect loading (headgear).

3.4 Finite element analysis simulation

The distributions of the contact pressures on the face obtained with direct loading is presented (**Figure 39**).

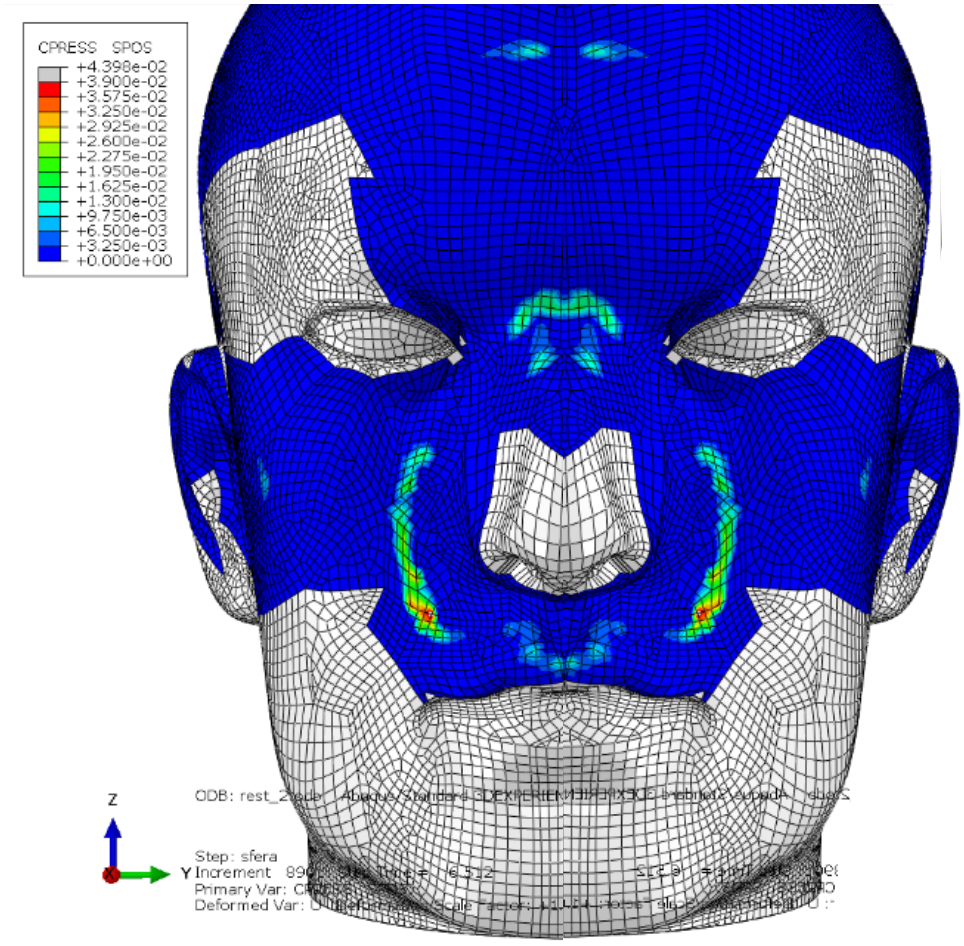

Figure 39 Distributions of contact pressures on the face for the direct loading.

The distributions of the contact pressures on the face obtained with direct loading of 20N is presented (**Figure 40**).

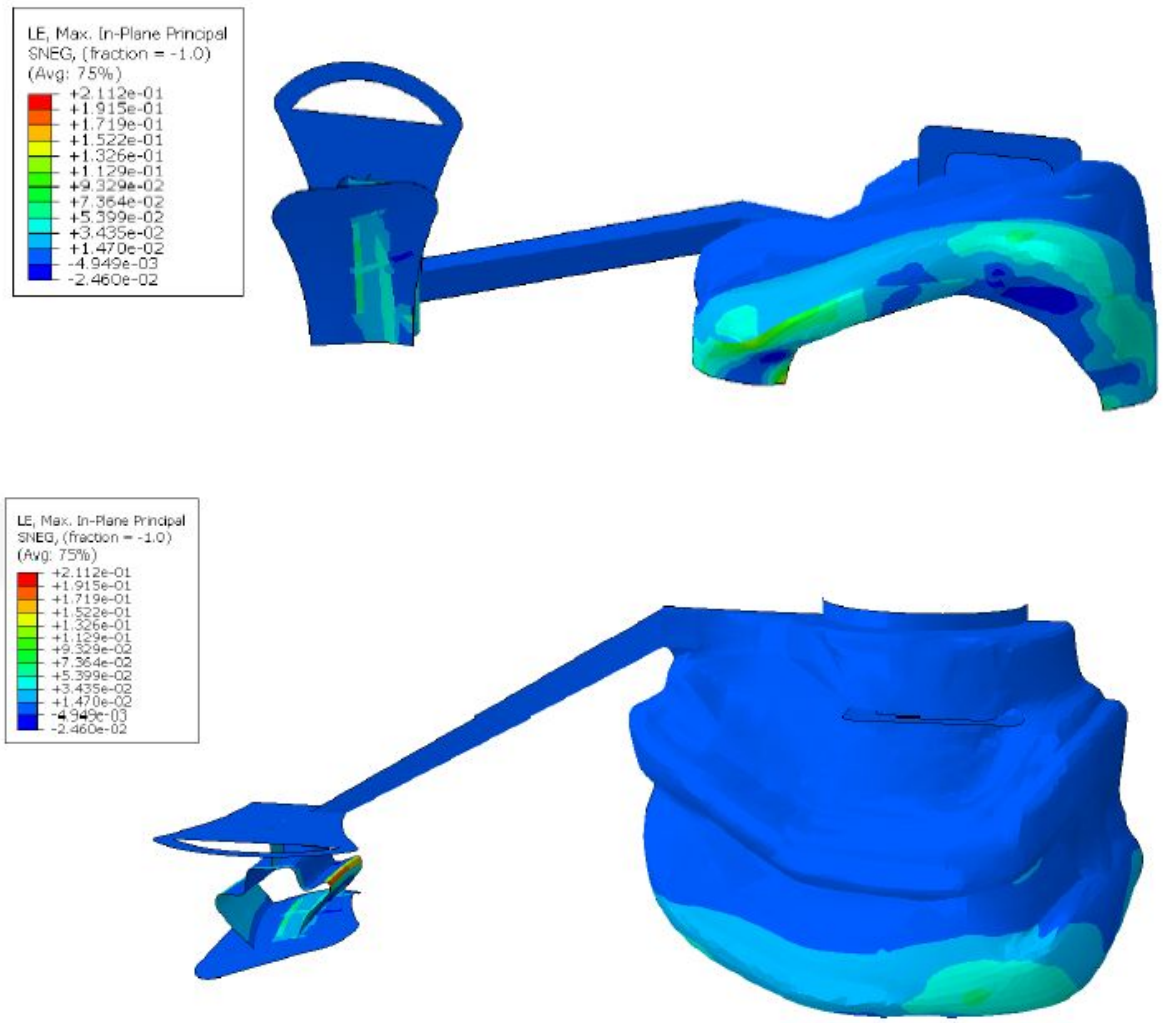

Figure 40: Distributions of contact pressures on the face for the direct loading.

3.5 Comparison between finite element analysis simulation and in-vitro experiment

The FEA produced, within the limitations due to assumptions and experimental conditions, results that were comparable with the experimental ones, regarding both the distribution of the pressures (**Figure 41** and **Figure 42**) and their magnitude (**Table 3**).

In particular, with regard to the force-displacement curves, the results with the direct loading were acceptable, but the one obtained with the headgear bands considerably depended on the characteristics of the bands (elastic modulus and inclination).

Whereas, the contact pressures were overlapping with the laboratory findings also when the headgear bands were used, regarding the shape of the contact surfaces, the location of the loaded areas, and the absolute values (same order of magnitude).

In general, the applied pressures were slightly lower in the FEA, and the most critical area seemed to be the maxilla. Such differences may vary based on the position of the mask in the FEA, and in the simulation obtained with indirect loading through the headgear bands the contact area shifted towards the forehead.

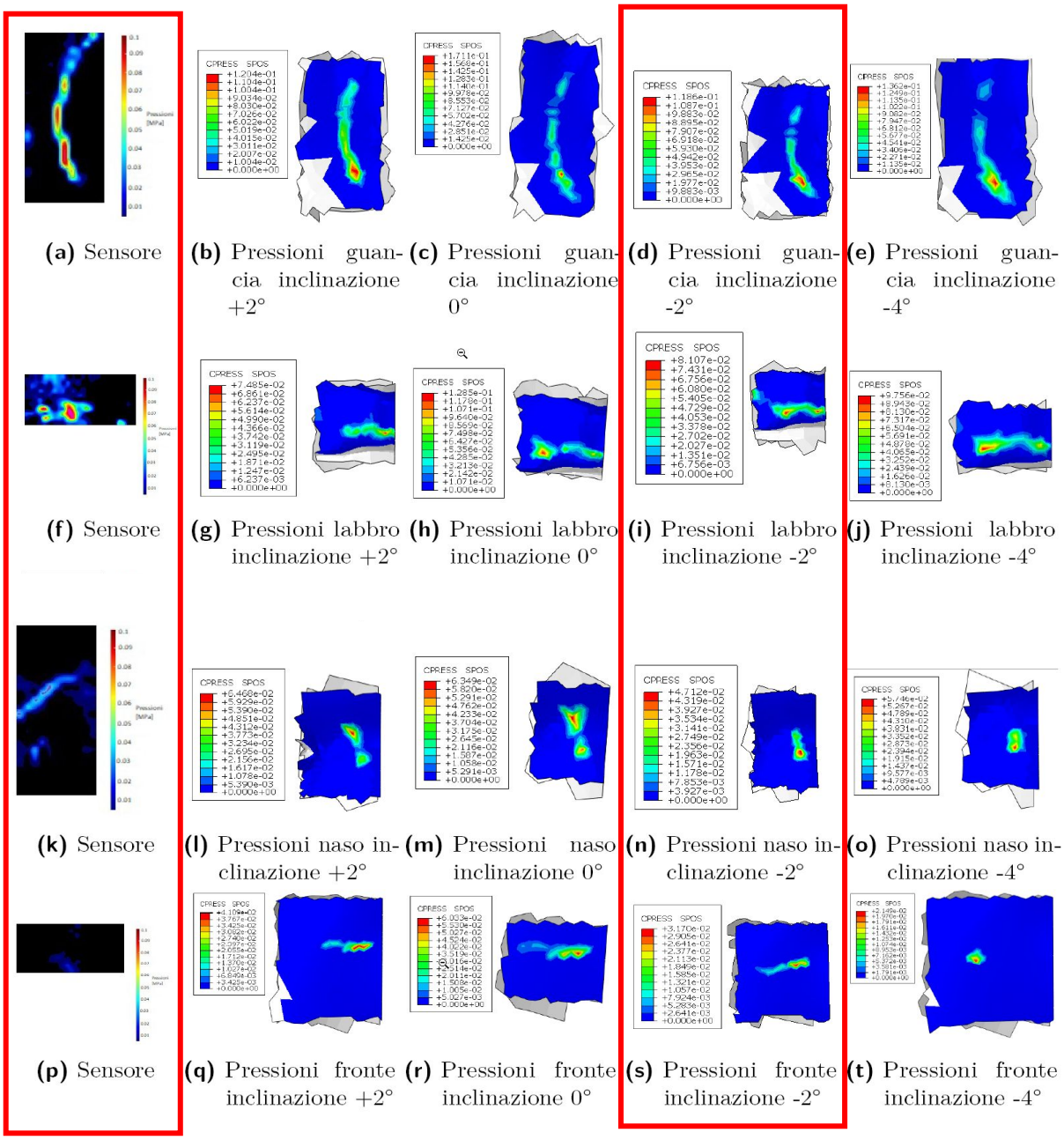

Figure 41: Distributions of contact pressures on the sensors (**left**) and simulated by the FEA (**right**), during the simulation with perpendicular loading (with different initial inclinations of the mask, that were +2°, 0°, -2°, and -4°). Similar findings are highlighted in red.

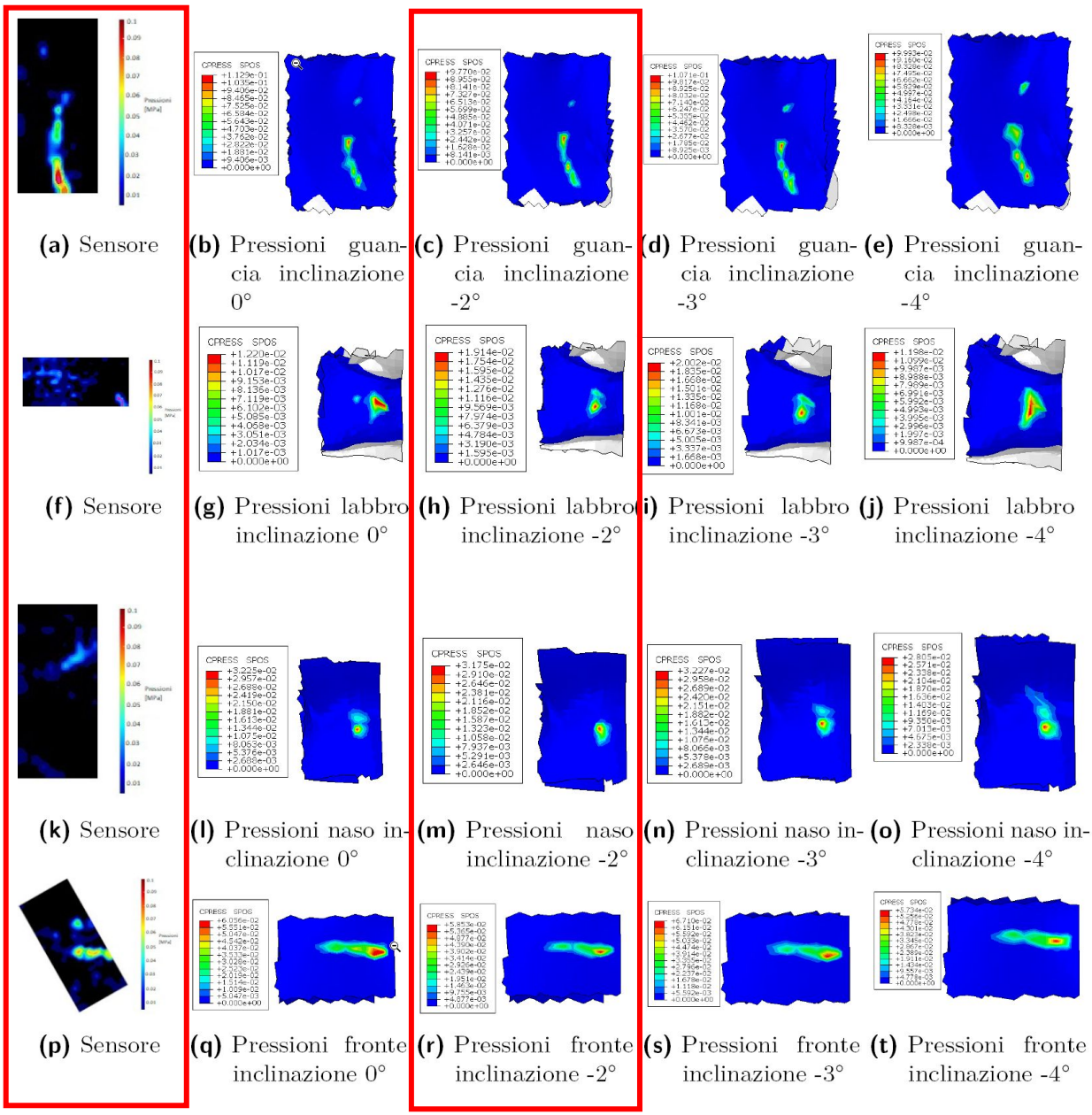

Figure 42: Distributions of contact pressures on the sensors (**left**) and simulated by the FEA (**right**), during the simulation with loading through the headgear bands (with different initial inclinations of the mask, that were 0°, -2°, -3°, and -4°). Similar findings are highlighted in red.

	Maximum pressure (MPa)				
	Direct loading (20N)				
	Exper	FEA +2°	FEA 0°	**FEA -2°**	FEA -4°
Forehead	**0.012**	0.041	0.050	**0.021**	0.012
Zygoma	**0.080**	0.120	0.100	**0.098**	0.110
Nasal bridge	**0.026**	0.048	0.052	**0.031**	0.033
Maxilla	**0.063**	0.049	0.085	**0.054**	0.073
	Loading with headgear bands (20N)				
	Exper	FEA +2°	FEA 0°	**FEA -2°**	FEA -4°
Forehead	**0.055**	0.060	0.058	**0.067**	0.057
Zygoma	**0.069**	0.075	0.065	**0.071**	0.074
Nasal bridge	**0.023**	0.032	0.031	**0.032**	0.028
Maxilla	**0.023**	0.012	0.020	**0.020**	0.012

FEA = finite element analysis

Table 3: Comparison of the maximum pressures obtained at 20 N either with direct loading or with loading with the headgear bands. Similar findings are highlighted in red.

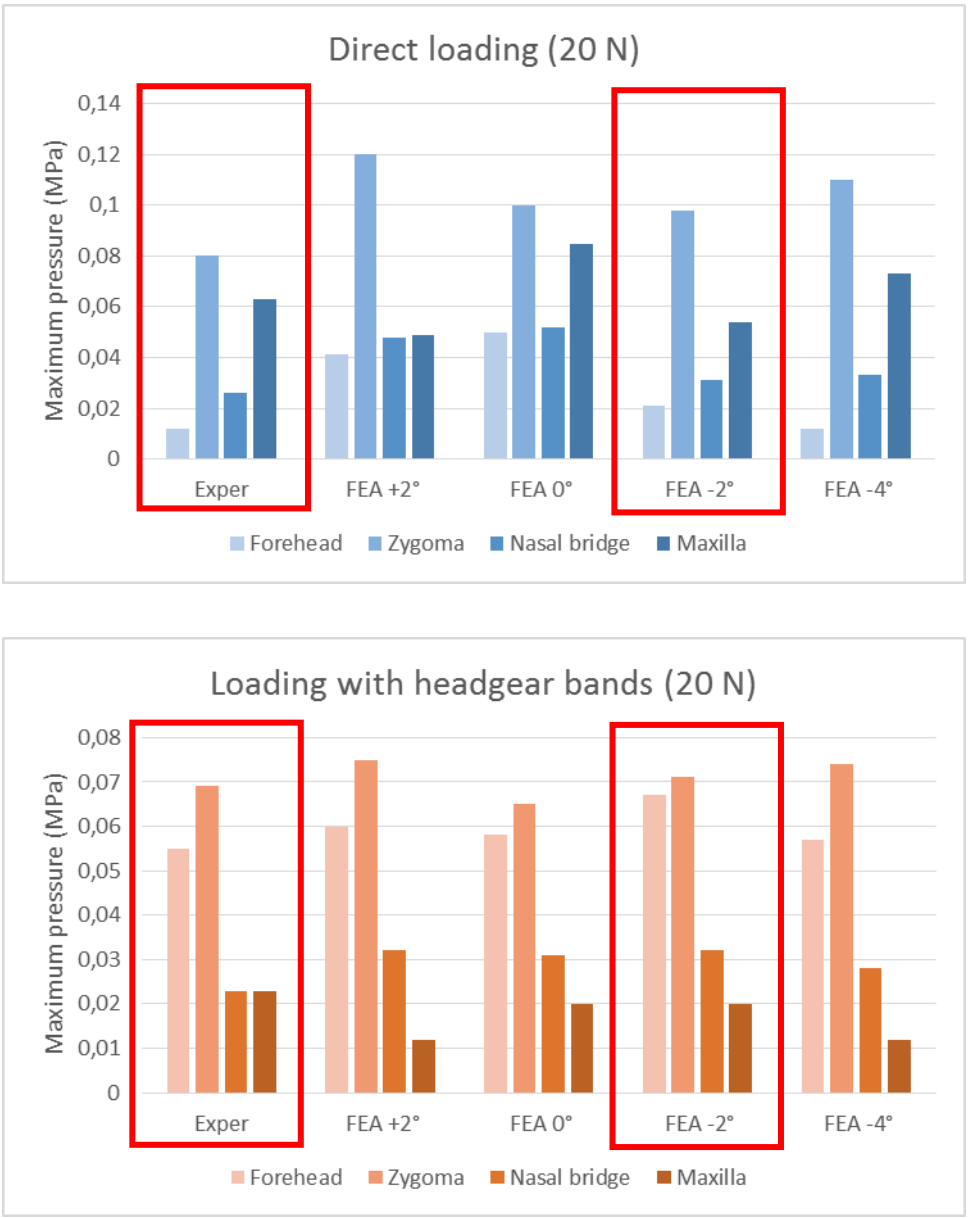

Figure 43: Comparison of the maximum pressures obtained at 20 N either with direct loading or with loading with the headgear bands. Similar findings are highlighted in red.

4. DISCUSSION

First of all, it was important to discuss the physiology of craniofacial biomechanics, in order to better understand the potential effects of the forces generated by the CPAP mask. Then, it was clarified what are the known effects, in terms of craniofacial growth, of long-term use of CPAP masks in growing patients. This allowed to better contextualise the results obtained from the FEA simulation and the in-vitro simulation under the clinical point of view. For validating the FEA model, it was also necessary to compare the FEA simulation and the mechanical testing. Lastly, it is noteworthy that the present experiments are among the first attempting to clarify the distribution of the forces of the CPAP on the face, and future studies are necessary to achieve a more realistic representation of the clinical scenario, especially with regard to multiple variables that were neglected in the present work.

4.1 Experimental part and simulation

Overall, while the FEA simulation with direct loading was relatively simple, the simulation including the headgear bands revealed a complex scenario. The complexity of such settings were attributable to large rigid movements, displacements, and deformations. In addition, the contact condition and the complicated geometry led to a large model accounting for multiple variables. Still, despite the long calculation time required to compute the FEA, an analysis of about one day allowed to achieve reasonable results that would otherwise require an excessive number of laboratory tests.

In general, the comparison of each area between the FEA and the laboratory experiment showed similar results *(Napoli, 2020)*. However, the most critical area seemed to be the upper lip, which showed a smaller loading in the FEA. Overall, the applied pressures were slightly lower in the FEA, but still within a similar order of magnitude. Such differences may vary based on the position of the mask adopted in the FEA. In particular, in the FEA obtained with indirect loading through the headgear, the contact area shifted towards the forehead. This said, the presented model may be used for providing an initial estimation of the forces and pressures exerted by the CPAP mask on the face. For the range of forces adopted, although the forces actually present during the clinical use of the CPAP mask are unknown, a wide range (from 5 N to 20 N) was used in the present study in order to cover the various hypothetical clinical scenario.

At present, little information is available on this topic. Recent studies carried directly on patients have described the pressures generated by the CPAP mask on facial areas such as the nasal bridge, ranging from 60 to 75 mm of Hg according to one study *(Brill, 2017a)*, and from 47 to 92 mm of Hg according to other authors *(Brill, 2017b)*. These values ranging from

6.27 to 12.27 kPa are in agreement with the average values obtained in the nasal area with a load between 5 and 20 N applied through the headgear, which ranged from 7.3 to 9.2 kPa. However, the average values obtained with direct loading were higher, ranging from 9.8 to 13.3 kPa.

Although forces of 0.5 N were reported on the cheeks, 2 N on the nasal bridge, and 4 N on the chin have been reported by others *(Cohen, 2018)*, the pressure values were not specified and a direct comparison with the present findings was not possible.

In addition, the present investigation provided data on multiple areas, including the forehead, the zygomatic area, the nasal bridge, and the upper jaw.

4.2 Physiology of craniofacial biomechanics

The human craniofacial skeleton is composed by rigid cranial and facial bones that may undergo remodelling either on their surfaces or along their articulations. Craniofacial sutures are articulation belonging to the category of the synarthrosis, which are immovable or nearly immovable articulations, and more specifically to the syndesmosis, fibrous articulation with a ligament between the parts (the sutural ligament) connecting the respective bones *(Savoldi et al., 2018a)*.

Sutures play a fundamental role in the shaping of the head during the growth process *(Enlow, 1990)*, and have a peculiar anatomy that varies according to the physiological stress that a certain region undergo *(Savoldi et al. 2019)*. In fact, their system is in synergic interaction with the craniofacial skeleton *(Rafferty et al., 1999)* during, for example, impacts *(Mouzakes et al., 1999)*, orthopaedic procedures *(Ghoneima et al., 2011)*, or mastication *(Maloul et al., 2012)*. Sutures are growth sites that can be stimulated by the application of forces *(Hierl et al., 2001)*, and the mid-face also includes sutures that can be loaded in order to obtain growth modifications, such as during rapid maxillary expansion *(Haas, 1965; Compadretti GC, 2006)*. Unfortunately, very few human sutures received biomechanical characterisation so far *(Savoldi et al. 2018a)*, and mechanical data are available for most sutures of swine *(Savoldi et al. 2017)*, with the maxillary sutures receiving particular attention *(Savoldi et al., 2018b)*.

4.3 Clinical considerations of the CPAP forces on the face

In growing patients, some case reports have given reason to hypnotise a causal relationship between use of CPAP masks and growth alterations leading to the development of retruded maxilla *(Li, 2000; Villa, 2002)*. In addition, other authors described an association between maxillary retrusion and longer daily use of NPPV in most of the subject undergoing CPAP *(Fauroux, 2005)*. However, a causal relationship has not been yet demonstrated.

Relatively to adult patients, prolonged use of CPAP mask may change some sagittal craniofacial and dental parameters, reducing jaws prominence and/or altering the inter-arch relationship *(Tsuda, 2010)*. Others compared dentofacial changes between mandibular advancement devices (MAD) and CPAP therapy, finding some statistically significant changes in dental inclination and facial height, but of negligible clinical interest (<0.6 º for angular measurements, and <0.2 mm for linear measurements), and no antero-posterior change was reported *(Doff, 2010)*.

Dentofacial orthopaedics is dealing with non-surgical growth modification since more than one century, and antero-posterior movement of the maxilla is studied since the 1960s *(Graber, 1985)*. Studies have focused mainly on the forward movement of the maxillary complex (for the treatment of mid-face hypoplasia), and fewer have analysed the backward displacement or the retention of a forward growth *(Braun, 2004)*.

Overall, a general agreement can be found saying that skeletal movement requires "heavy forces", probably in the range of 500 g to 1500 g *(Graber, 1985)*, or between 2 N and 12 N *(Braun, 2004; Johnson, 1999; Lyons, 2002)*. With regard to this, the primary growth modification is directed towards the upper jaw (maxilla), since the lower jaw (mandible) is attached to the cranium with a joint constituted by a condyle and a synovia that - if compressed

- causes necrosis. On the other hand, the maxilla is attached to the cranium with sutures, which properties have been described above. Thus, what clinically matter is that the forces on the mandible are not high enough to cause joint problems, and that the forces on the maxilla are not high enough to restrain the growth.

It is worth noting that the craniofacial skeleton grows until the age of 19-year-old, and that in earlier stages its susceptibility to orthopaedic forces is greater. Since CPAP treatments might be prescribed even earlier than dentofacial orthopaedic treatments, there is a legitimate concern of possible deformations of the craniofacial skeleton even at forces that usually do not reach skeletal deformation in elder subjects. In fact, since the maxillofacial complex tend to complete most of its growth around twelve years, previous authors suggested to avoid prolonged CPAP therapy below that age *(Villa et al.)*. In addition, the growth of the neurocranium can proceed till seven years, and further attention should be paid to young children wearing headgears bends loading the calvaria as well.

The growth of the maxilla and of the mandible occurs in different periods, as the sutures finish to grow at about 17-year-old, while condyles may grow up to 19-year-old. The pressure generated by the CPAP can have different effects depending on the predisposition of specific anatomical areas to undergo bone resorption. Thus, it was important to assess the distribution of the forces in different areas, and the simulation and experimental tests showed that the CPAP mask can exert forces that are not uniformly distributed on the face.

In general, it is suggested to use a headgear system that, compared to the one analysed in the present study, decreases pressures of the zygomatic area, possibly by redirecting those pressure on the forehead. In fact, forehead growth is less affected by orthopaedic forces compared to the midfacial growth. Furthermore, a less prominent forehead my not have negative effects on nasal breathing that are related to midface hypoplasia instead.

The directional forces of several types of headgears have been carefully analysed by orthodontists in the past century *(Graber, 1985)*. Similar concepts should be applied to the forces generated by wearing the CPAP mask, and a scrupulous evaluation of action on active sites and reactions on anchorage areas shall be performed. Interpretation of the presented mechanical data with respect to craniofacial biomechanics should be considered by clinicians in order to obtain the best compromise between the CPAP treatment performance - in terms of ventilation - and the possible side-effects on growing craniofacial structures.

4.4 Limitations

Regarding the numerical part, the two major issues of the system were the geometries (in terms of complexity), the contacts (as it was difficult to establish the most meaningful initial contact), and the big displacements, which complicated the calculation. In addition, the head was considered as completely rigid, which may have affected the contact areas and pressures compared to a CPAP mask positioned on soft skin. Sensors were also rigid, and light pressures were challenging to be detected.

Furthermore, a series of variables may affect the distribution of the forces of the CPAP mask on the face, such as the CPAP mask size (small, medium, large), the CPAP mask type (nasal, oral, oro-nasal mask), the direction of the headgear (high, medium, low). In the present study, only one head, with one CPAP mask, and one headgear orientation were simulated. Even though in the present experiment only one size of CPAP was used, the presence of a proportional distribution of the pressures could be assumed, as smaller CPAP are used on patients with smaller head, and larger CPAP are used for patients with larger head.

In addition, patient variables may also play a role, such as skeletal class (I, II, III), and age that also affects the size of the head.

Lastly, it is noteworthy that no air pressure applied, *i.e.* the CPAP mask was not tested during connection to the CPAP machine, which may influence the force distribution.

Overall, the present study did not aim at suggesting clinical guidelines for the treatment of growing patients with OSA *(Gu et al. 2020)*, and the presented results should be interpreted with caution when related to decision making in the treatment planning.

4.5 Future developments

With regard to the clinical validity of the FEA, future studies may include facial soft tissues to simulate the presence of the skin (which may have a relevant role in the contact pressures), and craniofacial sutures in the head model (which are interesting in terms of effects of the pressures on the craniofacial growth). Such variables would be challenging to simulate in mechanical testing, and their inclusion in the FEA would be appropriate.

Considering the numerical aspects of the FEA, the adopted mesh may be optimised, by comparing a denser mesh with a more discrete one, and assessing whether such difference also affects the FEA findings. In addition, the shell elements might be abandoned in favour of a 3D model of the VMQ parts, which would require an accurate 3D geometry of such components.

Further researches may also consider younger age groups. In fact, infants treated with naso-tracheal intubation for a period of one day to five weeks, nasal deformities were correlated with prolonged intubation (longer than five days), while no nasal deformities developed in patient ventilated for less than six days *(Gowdar, 1980)*. Similarly, infants using flow driver continuous positive airway pressure (a modified naso-tracheal tube which permitted prolonged intermittent positive pressure ventilation) for a period of 6 months was associated with snubbing of the nose, flaring of the nostrils and columella nasi necrosis which can progress to include septal necrosis *(Robertson, 1996)*. Furthermore, 6% of new-born babies using CPAP with an intubation period from four days to 46 days had deformities such as stenosis of the nares and septal erosion *(Baxter, 1975)*.

Furthermore, future clinical trials may compare different types of masks on the basis of the most significant variables highlighted by the model developed in the present study.

Lastly, the simulation presented in this work may contribute to medical teaching in the specific fields of craniofacial orthopaedics and sleep medicine. In fact, 3D models are relevant in medical education *(Savoldi et al. 2020a)*, and dynamic simulations may have a relevant role for the understanding of complex phenomena involving non-static tissues and active medical devices.

5. CONCLUSIONS

5.1 Virtual simulation

The developing of a FEA of the contact pressures generated by the application of a CPAP mask on the face seems to be feasible. Within the limitations of the present work, the FEA model allowed to estimate contact pressures and contact areas in different facial regions of clinical interest. The position of the mask and the characteristics of the headgear used to secure the mask on the face seem to be the most relevant variables.

5.2 Clinical relevance

Our simulation and laboratory assessment showed that CPAP masks can exert forces that are not uniformly distributed on the face. In particular, forces may be concentrated in the maxillary region, which growth may be affected. Thus, the design of the CPAP mask and, especially, of the headgear should be oriented to re-distribute the forces on less relevant regions such as the forehead. A careful evaluation of craniofacial biomechanics should be performed by clinicians in order to obtain the best compromise between maximising the CPAP performance in terms of ventilation and the possible side-effects on the living tissues.

6. REFERENCES

1. American Academy of Sleep Medicine. (2008). Clinical guidelines for the manual titration of positive airway pressure in patients with obstructive sleep apnea. *Journal of Clinical Sleep Medicine*, 4(2), 157.

2. Bartolucci ML, Bortolotti F, Raffaelli E, D'Antò V, Michelotti A, Alessandri Bonetti G. (2016). The effectiveness of different mandibular advancement amounts in OSA patients: a systematic review and meta-regression analysis. *Sleep and Breathing*, 20(3), 911-919.

3. Baxter RJ, Johnson JD, Goetzman BW, Hackel A. (1975). Cosmetic Nasal Deformities Complicating Prolonged Nasotracheal Intubation in Critically III Newborn Infants. *Pediatrics,* 55(6):884-887.

4. Bower A. F. Applied Mechanics of Solids. (2009). CRC Press.

5. Braun S, Bottrel, JA. (2004). Pilot study evaluating the effects of a cervical headgear on the C-axis: The growth axis of the dentomaxillary complex. *American Journal of Orthodontics and Dentofacial Orthopedics*, 126(6), 694-698.

6. Brill AK, Moghal M, Morrell MJ, Simonds AK. (2017). Randomized crossover trial of a pressure sensing visual feedback system to improve mask fitting in noninvasive ventilation. *Respirology*, 22(7), 1343-1349.

7. Brill AK, Pickersgill R, Moghal M, Morrell MJ, Simonds AK. (2018). Mask pressure effects on the nasal bridge during short-term noninvasive ventilation. *ERJ Open Research*, 4(2).

8. Chan J, Edman JC, Koltai PJ. (2004). Obstructive sleep apnea in children. *American Family Physician*, 69(5):1147-1160.

9. Compadretti GC, Tasca I, Alessandri Bonetti G. (2006). Nasal airway measurements in children treated by rapid maxillary expansion. *American Journal of Rhinology*, 20(4): 385-393.

10. Deng J, Gao X. (2012). A case–control study of craniofacial features of children with obstructed sleep apnea. *Sleep and Breathing*, 16(4), 1219-1227.

11. Doff MH, Hoekema A, Pruim GJ, Slater JH, Stegenga B. (2010). Long-term oral-appliance therapy in obstructive sleep apnea: a cephalometric study of craniofacial changes. *Journal of Dentistry,* 38(12):1010-1118.

12. Duran J, Esnaola S, Rubio R. Obstructive sleep apnea-hypopnea and related clinical features in a population-based sample of subjects aged 30 to 70 yr. (2001). *American Journal of Respirology and Critical Care Medicine*, 163: 685-689.

13. Enlow DH. Facial growth. WB Saunders Company, 1990.

14. Fauroux B, Lavis JF, Nicot F, Picard A, Boelle PY, Clément A, Vazquez MP. (2005). Facial side effects during noninvasive positive pressure ventilation in children. *Intensive Care Medicine*, 31(7):965-969.

15. Flores-Mir C, Korayem M, Heo G, Witmans M, Major MP, Major PW. (2013). Craniofacial morphological characteristics in children with obstructive sleep apnea syndrome: a systematic review and meta-analysis. *The Journal of the American Dental Association*, 144(3), 269-277.

16. Frohberg U, Naples RJ, Jones DL. (1995). Cephalometric comparison of characteristics in chronically snoring patients with and without sleep apnea syndrome. *Oral Surgery, Oral Medicine, Oral Pathology, Oral Radiology and Endodontics*, 80(1):28-33.

17. Gautam P, Valiathan A, Adhikari R. (2009). Craniofacial displacement in response to varying headgear forces evaluated biomechanically with finite element analysis. *American Journal of Orthodontics and Dentofacial Orthopedics*, 135(4), 507-515.

18. Ghoneima A, Abdel-Fattah E, Hartsfield J, El-Bedwehi A, Kamel A, Kula K. (2011) Effects of rapid maxillary expansion on the cranial and circummaxillary sutures. *American Journal of Orthodontics and Dentofacial Orthopedics*, 140(4):510-519.

19. Goldstein NA, Pugazhendhi V, Rao SM, Weedon J, Campbell TF, Goldman AC, Post JC, Rao M. (2004). Clinical assessment of pediatric obstructive sleep apnea. *Pediatrics*, 114(1):33-43.

20. Gowdar K, Bull MJ, Schreiner RL, Lemons JA, Gresham EL. (1980). Nasal deformities in neonates: Their occurrence in those treated with nasal continuous positive airway pressure and nasal endotracheal tubes. *American Journal of Diseases of Children,* 134(10):954-957.

21. Graber TM, Rakosi T, Petrovic AG. (1985). Dentofacial orthopedics with functional appliances (Vol. 2). St. Louis: Mosby.

22. Gu M, Savoldi F, Chan EYL, Tse CSK, Lau MTW, Wey MC, Hägg U, Yang Y. (2020). Changes in the upper airway, hyoid bone, and craniofacial morphology between the headgear activator and the Herbst appliance: a retrospective study on lateral cephalometry. *Orthodontics and Craniofacial Research*.

23. Guarnipol. Fabbrica guarnizioni e aricoli tecnici Guarnipol. Elastomeri, classificazioni, caratteristiche principali e compatibilità chimiche.

24. Gungor AY, Turkkahraman H, Yilmaz HH, Yariktas M. (2013). Cephalometric comparison of obstructive sleep apnea patients and healthy controls. *European Journal of Dentistry*, 7(1):48.

25. Haas AJ. (1065) The treatment of maxillary deficiency by opening the midpalatal suture. *The Angle Orthodontist*, 35:200-217.

26. Hedner J, Grote L, Bonsignore M, McNicholas W, Lavie P, Parati G, Sliwinski P, Barbé F, De Backer W, Escourrou P, Fietze I. (2011). The European sleep apnoea database (ESADA): report from 22 European sleep laboratories. *European Respiratory Journal,* 38(3):635-642.

27. Hierl T, Kloppel 410R, Hemprich A. (2001). Midfacial distraction osteogenesis without major osteotomies: a report on the first clinical application. *Plastic and Reconstructive Surgery,* 108(6):1667-1672.

28. Hultcrantz E, Tideström BL. (2009). The development of sleep disordered breathing from 4 to 12 years and dental arch morphology. *International Journal of Pediatric Otorhinolaryngology*, 73(9):1234-41.

29. Incerti Parenti S, Aroni E, Laffranchi L, Paganelli C, Alessandri-Bonetti G. (2020). The effectiveness of mandibular advancement devices in the treatment of obstructive sleep apnoea in adults: a methodological quality assessment of systematic reviews. *European Journal of Orthodontics*, 42(5), 483-493.

30. Instron. Ultra High and Precision Testing. Microelectronics testing solutions catalogue.

31. Jennum P, Kjellberg J. (2011). Health, social and economical consequences of sleep-disordered breathing: a controlled national study. *Thorax*, 66(7):560-566.

32. Jennum P, Riha RL. (2009). Epidemiology of sleep apnoea/hypopnoea syndrome and sleep- disordered breathing. *European Respiratory Journal*, 33: 907–909.

33. Johnson PD, Bar-Zion Y, Taylor M, Wheeler TT. (1999). Effects of head posture on headgear force application. *Journal of Clinical Orthodontics*, 33, 94-97.

34. Krieger J. (1992). Long-term compliance with nasal continuous positive airway pressure (CPAP) in obstructive sleep apnea patients and nonapneic snorers. *Sleep*, 15(suppl_6):S42-s46.

35. Leger P, Bedicam JM, Cornette A, Reybet-Degat O, Langevin B, Robert D, Polu JM, Jeannin L. (1994). Nasal intermittent positive pressure ventilation: long-term follow-up in patients with severe chronic respiratory insufficiency. *Chest*, 105(1):100.

36. Li KK, Riley RW, Guilleminault C. (2000). An unreported risk in the use of home nasal continuous positive airway pressure and home nasal ventilation in children: mid-face hypoplasia. *Chest*, 117(3), 916-918.

37. Lightowler JV, Wedzicha JA, Elliott MW, Ram FS. (2003). Non-invasive positive pressure ventilation to treat respiratory failure resulting from exacerbations of chronic obstructive pulmonary disease: Cochrane systematic review and meta-analysis. *British Medical Journal*, 326(7382):185.

38. Löfstrand-Tideström B, Thilander B, Ahlqvist-Rastad J, Jakobsson O, Hultcrantz E. (1999). Breathing obstruction in relation to craniofacial and dental arch morphology in 4-year-old children. *The European Journal of Orthodontics*, 21(4):323-332.

39. Lyons EK, Ramsay DS. (2002, March). Preliminary tests of a new device to monitor orthodontic headgear use. In Seminars in Orthodontics (Vol. 8, No. 1, pp. 29-34). WB Saunders.

40. Maloul A, Regev E, Whyne CM, Beek M, Fialkov JA. (2012) In vitro quantification of strain patterns in the craniofacial skeleton due to masseter and temporalis activities. *Journal of Craniofacial Surgery*, 23(5):1529-1534.

41. Massie CA, McArdle N, Hart RW, Schmidt-Nowara WW, Lankford A, Hudgel DW, Douglas NJ. (2003). Comparison between automatic and fixed positive airway pressure

therapy in the home. *American Journal of Respiratory and Critical Care Medicine*, 167(1), 20-23.

42. Mcardle N, Devereux G, Heidarnejad H, Engleman HM, Mackay TW, Douglas NJ. (1999). Long-term use of CPAP therapy for sleep apnea/hypopnea syndrome. *American Journal of Respiratory and Critical Care Medicine,* 159(4):1108-1114.

43. Mortimore IL, Whittle AT, Douglas NJ. (1998). Comparison of nose and face mask CPAP therapy for sleep apnoea. *Thorax*, 53(4), 290-292.

44. Mouzakes J1, Koltai PJ, Simkulet MD, Castracane J. (1999). Evaluation of orbital stress dissipation in pediatric and adult skulls using electronic speckle pattern interferometry. *Archives of Otolaryngology and Head and Neck Surgery*, 125(7):765-773.

45. Napoli E. Modellazione numerica del trattamento delle apnee del sonno con ventilazione meccanica a pressione positive continua (Cpap). (2020). Thesis for the Master Degree in Civil Engineering. University of Brescia, Brescia, Italy.

46. Oto J, Li Q, Kimball WR, Wang J, Sabouri AS, Harrell PG, Kacmarek RM, Jiang Y. (2013). Continuous positive airway pressure and ventilation are more effective with a nasal mask than a full face mask in unconscious subjects: a randomized controlled trial. *Critical Care,* 17(6):R300

47. Pae EK, Ferguson KA. (1999). Cephalometric characteristics of nonobese patients with severe OSA. *The Angle Orthodontist*, 69(5):408-12.

48. Peko Cohen L, Ovadia-Blechman Z, Hoffer O, Gefen A. (2019). Dressings cut to shape alleviate facial tissue loads while using an oxygen mask. *International Wound Journal,* 16(3), 813-826.

49. Pirilä-Parkkinen K, Pirttiniemi P, Nieminen P, Tolonen U, Pelttari U, Löppönen H. (2008). Dental arch morphology in children with sleep-disordered breathing. *The European Journal of Orthodontics*,31(2):160-167.

50. Rafferty KL, Herring SW. (1999). Craniofacial sutures: morphology, growth, and in vivo masticatory strains. *Journal of Morphology*, 242(2):167.

51. Robertson NJ, McCarthy LS, Hamilton PA, Moss AL. (1996). Nasal deformities resulting from flow driver continuous positive airway pressure. *Archives of Disease in Childhood-Fetal and Neonatal Edition*, 75(3):F209-F212.

52. Rosen CL. (2010). Obstructive sleep apnea syndrome in children. In ACCP/AAP Pediatric Pulmonary Board Review: 1st Edition. *American College of Chest Physicians*.

53. Savoldi F, Massetti F, Tsoi JKH, Matinlinna JP, Yeung AWK, Tanaka R, Paganelli C, Bornstein MM. (2020). The antero-posterior length of the maxillary complex and its relationship with the anterior cranial base: A study on human dry skulls using cone beam computed tomography (CBCT). *The Angle Orthodontist.* (c)

54. Savoldi F, Tsoi JKH, Paganelli C, Matinlinna JP. (2017). Biomechanical behaviour of craniofacial sutures during distraction: An evaluation all over the entire craniofacial skeleton. *Dental Materials*, 33(7):e290-e300.

55. Savoldi F, Tsoi JKH, Paganelli C, Matinlinna JP. (2018). The biomechanical properties of human craniofacial sutures and relevant variables in sutural distraction osteogenesis: a critical review". *Tissue Engineering, Part B: Reviews*, 24(1):25-36. (a)

56. Savoldi F, Tsoi JKH, Paganelli C, Matinlinna JP. (2019). Sutural morphology in the craniofacial skeleton: a descriptive micro-computed tomography study in a swine model. *The Anatomical Record*, 302(12):2156-2163.

57. Savoldi F, Xinyue G, McGgrath CP, Yang Y, Chow SC, Tsoi JKH, Gu M. (2020), Reliability of lateral cephalometric radiography in the assessment of the upper airway in children: A retrospective study. *The Angle Orthodontist*, 90(1):47-55. (b)

58. Savoldi F, Xu B, Tsoi JKH, Paganelli C, Matinlinna JP. (2018). Anatomical and mechanical properties of swine midpalatal suture in the premaxillary, maxillary, and palatine region. *Scientific Reports*, 8(1):7073. (b)

59. Savoldi F, Yeung AWK, Tanaka R, Zadeh LSM, Montalvao C, Bornstein MM, Tsoi JKH. (2020). Dry skulls and cone beam computed tomography (CBCT) for teaching orofacial bone anatomy to undergraduate dental students. *Anatomical Sciences Education*. (a)

60. Smith DF, Dalesio NM, Benke JR, Petrone JA, Vigilar V, Cohen AP, Ishman SL. (2016). Anthropometric and dental measurements in children with obstructive sleep apnea. Journal of clinical sleep medicine: *Journal of Clinical Sleep Medicine*, 12(9):1279.

61. Tanne K, Matsubara S, Sakuda M. (1993). Stress distributions in the maxillary complex from orthopedic headgear forces. *The Angle Orthodontist*, 63(2), 111-118.

62. Tanne K, Matsubara S. (1996). Association between the direction of orthopedic headgear force and sutural responses in the nasomaxillary complex. *The Angle Orthodontist*, 66(2), 125-130.

63. Tsara V, Amfilochiou A, Papagrigorakis MJ, Georgopoulos D, Liolios E. (2009). Definition and classification of sleep related breathing disorders in adults: Different types and indications for sleep studies (Part 1). *Hippokratia*, 3(3):187.

64. Tsuda H, Almeida FR, Tsuda T, Moritsuchi Y, Lowe AA. (2010). Craniofacial changes after 2 years of nasal continuous positive airway pressure use in patients with obstructive sleep apnea. *CHEST Journal*, 138(4), 870-874.

65. Villa MP, Pagani J, Ambrosio R, Ronchetti R, Bernkopf E. (2002). Mid-face hypoplasia after long-term nasal ventilation. *American Journal of Respiratory and Critical Care Medicine*, 2166(8):1142-1143.

7. ACKNOWLEDGEMENTS

The author would like to thank Professor Corrado Paganelli (Dean of the Dental School, Department of Medical and Surgical Specialties, Radiological Sciences and Public Health, University of Brescia, Brescia, Italy) and Professor Nicola Francesco Lopomo (Department of Information Engineering, University of Brescia, Brescia, Italy), supervisors of this thesis, for their tutoring during all phases of the research work; Professor Francesco Genna (Department of Civil, Environmental, Architectural Engineering and Mathematics, University of Brescia, Brescia, Italy) and Dr. Fabio Savoldi (Orthodontics, Dental School, Department of Medical and Surgical Specialties, Radiological Sciences and Public Health, University of Brescia, Brescia, Italy) for the contribution to the study design, data collection, and data analysis; Professor Giorgio P. M. Vassena (Gexcel S.r.l., Brescia, Italy) for his contribution in the processing and analysis of the 3D geometries; Dr. Erica Napoli (Department of Civil, Environmental, Architectural Engineering and Mathematics, University of Brescia, Brescia, Italy) for the data collection and the numerical simulations; Professor Antonio Fiorentino and Dr. Gabriele Allegri (Department of Mechanical and Industrial Engineering, University of Brescia, Brescia, Italy) for the support with the 3D scanning of the phantom head and the CPAP mask; and the FCI Lab (Laboratorio di Fisiologia Clinica Integrativa, University of Brescia, Brescia, Italy) for providing the contact pressure-mapping system.